Research Report 2015–09

DEVELOPMENT OF PHYSICAL-EMPIRICAL MODELS FOR SEASONAL PREDICTIONS OF WINTERTIME CLIMATE VARIABLES OVER EAST ASIA

Vladimir Kryjov

APCC
APEC CLIMATE CENTER

Research Report 2015–09

DEVELOPMENT OF PHYSICAL-EMPIRICAL MODELS FOR SEASONAL PREDICTIONS OF WINTERTIME CLIMATE VARIABLES OVER EAST ASIA

Vladimir Kryjov

APCC
APEC CLIMATE CENTER

PREFACE

The recent years were marked by revival of the interest in empirical climate studies and statistical methods of seasonal climate prediction. It became clear that our existing knowledge is not sufficient for developing of dynamical climate models able to appropriately simulate the processes in the extratropical climate system. Meanwhile, physical-empirical methods provide insight into the main forcings and feedbacks, which define evolution of the climate system on the seasonal time scale. These methods provide the basis for increasing the reliability of seasonal forecasting as well as the improvement of dynamical climate models.

This year, APCC has begun a physical-empirical prognostic research activity in order to increase the reliability of seasonal predictions for East Asia. Physical-empirical models based on physically plausible empirically established mechanisms and statistical links complement dynamical model forecasts and enable further improvements of the dynamical models by accounting for the established mechanisms.

This research is focused on the one-month-lead seasonal prediction of wintertime temperature in East Asia. In particular, it investigates the system of forcings and feedbacks affecting the formation of seasonal air temperature anomalies and the reliable physically plausible and stable in time lead-lag relationships between the relevant components of the climate system. The obtained knowledge provides a basis for the development of physical-empirical models linking the East Asian wintertime temperature anomalies with the preceding autumn anomalies of the

relevant climate variables using statistical tools.

The main result from the study in 2015 is a set of the physical-empirical models for prediction of the wintertime index of the Arctic Oscillation and of the East Asia wintertime temperature anomalies, which are substantially based on the extratropical sources of predictability. These physical-empirical models are mutually complementary with the dynamical models mainly governed from the tropics and possess a prediction skill that exceeds the existing dynamical models. Implementation of the developed methods into the APCC operational practice is expected to provide an essential improvement of our winter seasonal predictions for the extratropics.

I would like to acknowledge the dedicated work of Dr. Vladimir Kryjov who together with Dr. Yoojin Kim have pioneered the field of physical-empirical prognostic research at APCC as well as the staff of APCC supporting this work. Also, I would like to note that the promising results from the performed research open the way for further physical-empirical prognostic studies at APCC.

Dr. **Chin-Seung Chung**, Director
APEC Climate Center
January 2016

ABSTRACT

Results from a study focusing on the development of physical-empirical models for prediction of East Asia wintertime temperature appropriate to APEC Climate Center (APCC) operational practices are presented in this report. The developed statistical tool, which is based on a multiple regression scheme with flexible construction of the predictors, has been proven efficient in the tests simulating real-time forecasts for 30 winters (1983/84–2012/13). The tests have shown the ability of the developed method to construct physically plausible predictors based on the fields of atmospheric and surface variables. Predictions of the wintertime Arctic Oscillation Index with the use of Z500 fields as a basis for predictor construction yield the skill in terms of temporal unadjusted correlation coefficient (TCC) > 0.60 and mean square skill score (MSSS) > 0.35. Prediction for East Asia comprising forecast of the leading principal components of the wintertime temperature anomalies with further composition of the predicted anomaly fields yields prevailing skill for South Korea characterized by TCC = 0.40–0.60 and MSSS = 0.20-0.30. Since the predictability underlying prediction for East Asia with the developed method mainly originates from extratropical processes, it is concluded that improvement can be achieved by combination of forecasts from the developed physical-empirical model with seasonal forecasts from dynamic models that are mainly governed by tropical sea surface temperature anomalies.

CONTENTS

1. INTRODUCTION

Seasonal predictions of meteorological variables for East Asia are challenging. Although there exists a general understanding of the processes that contribute to the climate of East Asia, long-range forecasts still require further study. Reliable dynamical model seasonal predictions for East Asia have not yet been achieved. Particularly, APEC Climate Center (APCC) multi-model ensemble (MME) predictions of DJF T2m are associated with correlations of only 0.1–0.3 (Min et al., 2014; APCC website), the World Meteorological Organization Lead Center (WMO LC) MME predictions are of a similar skill level, namely, 0.1–0.3 (Kim et al., 2015a). Nowadays, more and more attention is paid to physical-empirical models (also known as statistical models because they are based on the statistical tools) because of their potential ability to provide superior results (e.g., Wang et al., 2013).

The wintertime processes in East Asia have been investigated in many studies. Jhun and Lee (2004) have proposed an index for the East Asian winter monsoon (EAWM) that is based on the gradient in Z300 zonal wind velocity, and they have shown that enhancement of the EAWM (thus, leading to lower temperatures in Korea) is associated with the enhancement of the mid–upper troposphere East Asian trough; furthermore, enhancement of the Siberian High (SH) and Aleutian low appears to be forerun by enlarged autumn snowfall in the SH area (Watanabe and Nitta, 1999; Clark and Serreze, 2000). Wang et al. (2010) developed two EAWM indices based on surface air temperature (SAT) variability (N and S) and showed that wintertime temperature anomalies in the southern and northern East Asian monsoon areas are preceded by different autumn snow cover anomalies; they also found that significant relationships with the El Nino–Southern Oscillation (ENSO) are featured by only the southern EAWM mode. A possible explanation for the weak influence on the northern mode follows from the Pacific Decadal Oscillation (PDO) modulation of the ENSO impacts on East Asia temperature (EAT), as shown by Wang et al. (2008), with the effect being markedly noticeable during the PDO negative phase and negligible during the positive one.

The concept of snow impact has been explored in a number of studies, with the most advanced version, which combines the snow extent and SLP anomalies,

having been implemented as an operational scheme (Cohen et al., 2007); however, with undiscovered SLP predictors. In 2011, the snow extent-based predictor (Snow Extent Index) was replaced by another snow index, the Snow Advance Index, which characterizes the rate of snow extent increase. However, that index was not confirmed in recent seasonal prediction model runs and Peings et al. (2013) showed that the snow extent–wintertime circulation (particularly, the Arctic Oscillation) linear relationships vary strongly with time. Kryjov (2015) has shown that anomalies in both the snow extent and East Asian trough result from anomalous autumn cold/warm advection to East Asia. Another autumn predictor suggested for the EAWM is sea ice extent (concentration) in the Arctic (Chen et al., 2014) as well as in the northern parts of the North Pacific (Liu et al., 2007). A crucial impact on the EAWM is imparted by the SH, which is strongly affected by Ural blocking (Cheung et al., 2012), and it tends to change its anomaly sing to the opposite between October and December (Chang and Lu, 2012; Kryjov, 2015).

Gong et al. (2001) show the relationships between the EAWM and the Arctic Oscillation (AO), with the latter being closely related to the SH, and Jeong and Ho (2005) demonstrate relationships between the number/frequency of cold surges in East Asia with the phase of the AO. The recent study of Park and Ahn (2015) has shown that the AO impact on EAT is modulated by the western Pacific pattern (WPP), with the strongest effect being achieved when both the AO and WPP are in their positive or negative phases. When their phases are opposite, the effect is weak. This modulation may explain the comparatively low (about 0.4) correlation between EAT and the AO Index. Meanwhile, a combination of the impacts of the AO and WPP by means of multiple regression results in a correlation of 0.65.

Notably, the above named studies do not go beyond basic descriptions of the relationships, and thus, the development of predictive models needs further work. A prediction scheme has been suggested by Lee et al. (2013), who developed a method for physical-empirical predictions of wintertime EAT based on their predictable modes. While their analysis demonstrate very good skill for the winters of 1981/82–2001/02 in cross-validation mode, assessment with independent forecasts shows strong degradation in the skill (which is typical when transitioning from an assessment based on dependent (fitting) or semi-dependent (cross-validated)

data to an assessment based on independent data). This decrease is caused by instability of the relationships associated mainly with the variations in the locations of predictors and the non-stationarity of the statistics of the time series.

This study is focused on the development of physical-empirical models for East Asia based on physically plausible relationships, with verification tests being performed on retrospective forecasts estimated by using a procedure of real-time forecasting with no influence from "future" years. The main goal of this study is to improve the predictions of wintertime temperature for East Asia, particularly, South Korea, based on advances in our understanding of East Asian climate forcings and feedbacks affecting the wintertime climate system.

The study is organized as follows. Section 2 briefly describes the data used in this study and the applied methodology for forecasting and verification; detailed descriptions of the developed forecasting technology and applied verification strategies are given in the Appendices. Section 3 covers the main research results. Particularly, Section 3.1 starts with a pre-forecasting analysis of the statistical relationships between wintertime South Korea temperature (DJF KST) and October and DJF variables so as to construct a general understanding of the autumn–winter climate system and to guide selection of the potential predictors for DJF KST. Then, the developed forecasting technology is tested with predictions of the wintertime AO Index, and these results are presented in Section 3.2. Section 3.3 presents the results of tests for the predictions of the DJF KST. Results from the supporting study on forecasting the EAWN indices are shown in Section 3.4. Section 3.5 presents the results of tests of the predictions of wintertime monthly temperature and seasonal total precipitation. The conclusions are presented in Section 4.

2. DATA AND METHODOLOGY

2.1 Data

For a target variable, we use temperature from the University of East Anglia (UEA) Climatic Research Unit (CRU) dataset, which consists of land only temperature and precipitation gridded on 0.5° × 0.5° mesh (Harris et al., 2014). South Korea temperature (KST) is represented by the land only temperature time series from the gridpoints within the trapezoid 38°N–34°N, 125°E–130°E. The Korea Peninsula temperature (KPT) trapezoid is expanded northward up to the 40°N parallel. East Asia temperature is represented by the land only series from the trapezoid 50°N–20°N, 100°E–150°E.

As predictors, we test variables from various sources. Circulation characteristics are represented by the SLP, geopotential heights, and zonal and meridional wind velocity from the National Centers for Environmental Prediction (NCEP)/National Center for Atmospheric Research (NCAR) Reanalysis 1 project (Kalnay et al., 1996). Sea surface properties, sea surface temperature (SST), and sea ice concentration (SIC) on a 1° × 1° grid were obtained from the UK Met Office (UKMO) Hadley Centre (Rayner et al., 2003)). Snow cover (SC) was taken from the 20th Century Reanalysis project (Whitaker et al., 2004; Compo et al., 2006; Compo et al., 2011). For illustrations of synoptic phenomena associated with the obtained correlation patterns, we use precipitation and temperature (T2m) from the above named 20th Century Reanalysis and Reanalysis 1 projects, respectively. The period for empirical study covers 1958/59–2012/13 (55 winters). In this report, we mark the winters by the year in which January falls, so our series is designated as 1959–2013.

2.2 Methodologies

Our forecasting methodology is based on self-tuning physical-empirical models employing multiple regression as a statistical tool. The main shortcoming of statistical models, particularly regression-based ones, is their inherent inability to predict extremes (e.g., Wilks, 1995) given that the underlying regression minimizes the mean

squared error (squared difference between the original and "reconstructed" series) from the training period. So that, even within a training period, the reconstructed predictand variance will be less than the original predictand variance, and it is equal to the latter multiplied by the squared correlation coefficient between the predictand and predictor. The predictand variance is even less for the forecast period (beyond the training period) because the data from the forecast period do not participate in the derivation of the regression equation.

We use two strategies for verification. The first involves simulation of the real-time forecasts. Another involves three-year-leave-out cross-validation. Because of the short training periods used (e.g., 25 years and 22 years for the real-time and cross-validated forecast procedures, respectively), the number of predictors should not exceed two. In the procedure simulating that of a real-time forecast, we operate with 26-year samples (series), with 25 years of which being used for training and the data from the 26^{th} year being used to validate the forecast. Throughout the whole assessment, training years always preceded the year of the forecast (in contrast to the cross-validation procedure in which the training period may cover the years after the year of the forecast).

Cross-validation is based on the assumption that time series are samples with no time order. To what degree it matches the natural environment and is applicable to statistical predictions is rather questionable, especially when accounting for long-range variability and trends for recent decades. However, since the series of Korea wintertime temperature are not (statistically) homogeneous, we use this approach with a three-year-leave-out as a supporting analysis technique to compare with the real-time mode performed on the "after shift" short series covering 1988–2012.

Detailed explanations of the forecasting and verification procedures are posted in Appendix 1 and Appendix 2, respectively.

3. RESEARCH RESULTS

3.1 South Korea Wintertime Temperature: Relationships and Pre-Prediction Analysis

3.1.1 South Korea Temperature Time Series Peculiarities

Time series of wintertime (December – February, DJF) temperature averaged over South Korea (KST) is shown in Figure 3.1.1. The mean value is -0.65°C, the standard deviation is 1.19°C. The main peculiarity strongly affecting the statistical simulation of the series is the lack of "cold" winters between 1986 and the early 2010s.

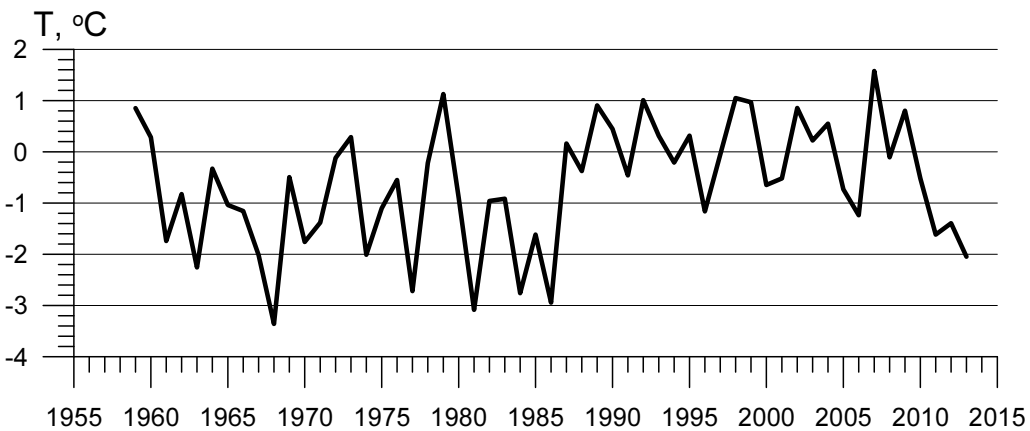

Figure 3.1.1 Time series of DJF air temperature averaged over South Korea (land only temperature from the trapezoid 38°N–34°N, 125°E–130°E). Years as of January.

The shift in means between the 27-year period for 1987–2013 and the preceding 27 years (1960–1986) is 1.2°C, with the corresponding Student's *t* statistic based on a parametric test being 5.99, and the based on the Mann–Whitney nonparametric test normally distributed *z* statistic being 3.68 (the Mann–Whitney nonparametric test is more conservative than the conventional parametric test). Time series of *t* and *z* statistics for the differences in means of the sliding 15-year neighbor windows are shown in Figure 3.1.2. Increase of the means is detectable throughout almost

the whole period, and the most essential increase is significant at the 99% confidence level; this occurs during the second half of the 1980s and the early 1990s. It may deteriorate forecasts because of inhomogeneity of predictand time series during training periods.

Wintertime monthly temperature time series are shown in Figure 3.1.3. The above mentioned shift between the winters of 1986 and 1987 is the strongest for the January series, and it is weaker but still noticeable in the February and December temperature series. It should be noted that this shift is also detectable in station time series datasets and has been described in the literature (e.g., Lee et al., 2013b).

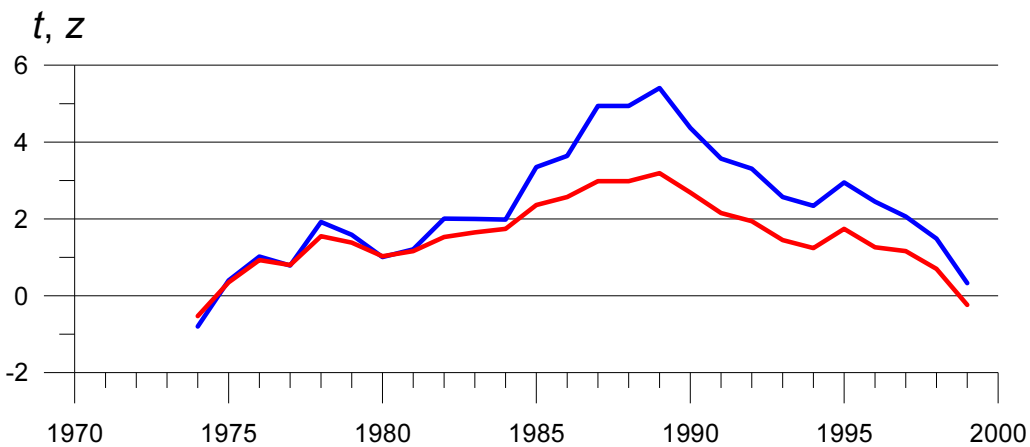

Figure 3.1.2 Statistical significance of the differences in means between the sliding 15-year neighbor windows of DJF air temperature averaged over South Korea. Blue – Student's t statistic based on parametric tests; red – z statistic based on Mann-Whitney tests.

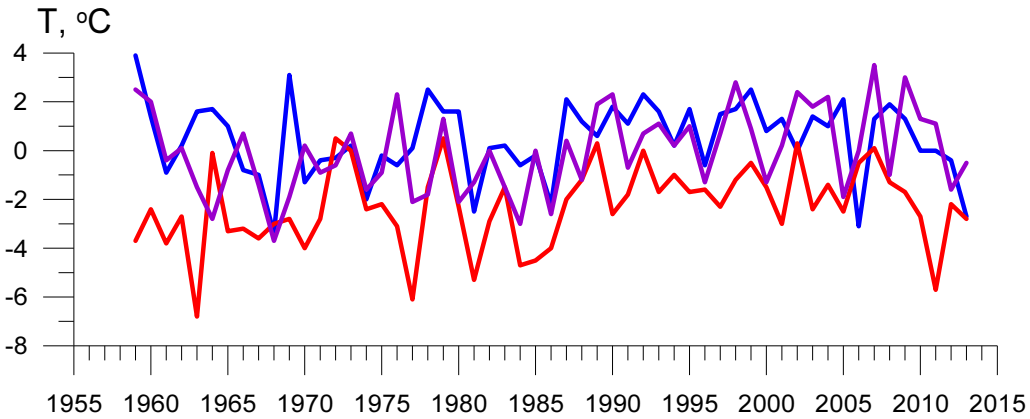

Figure 3.1.3 Time series of December (blue), January (red), and February (purple) air temperature averaged over South Korea. Years as of January; December temperature is marked on the next year.

Thus, the series of wintertime temperatures for the region are not statistically homogeneous. Between the winters of 1986 and 1987, there occurred a discontinuity; at least, in the statistical sense. In climatological sense, this discontinuity could be treated in two ways. The first is to treat the discontinuity as a short-term evolution within a long-range unresolved variability, e.g., a decadal-scale quasi-periodic process, with the status of the climate system being kept unchanged. Another way suggests that the discontinuity marks a climatological shift from one climatological status to another, which may imply an essential change in forcings and feedbacks. Practically, in our research, this alternative suggests two alternative methodological approaches. The first implies that we could consider the data from the whole available period as a single sample. The second implies that our series consists of two separated samples taken from different populations.

Discontinuity between the winters of 1986 and 1987 resides in the shift (at least statistical) toward warmer winters, or more accurately, to the lack of cold winters. Development and verification assessment of forecasting methods similar to those applied in the real-time mode forecasting requires long series since a training period in such an approach precedes a forecast year. That is, if the reasonable minimum length of the training period is 25 years and verification assessment is performed on not less than 30 forecasts, the whole series size should be not less than 55 years. Meanwhile, the temperature shift of 1986–1987 appears almost in the middle of the available 55-year series of 1959–2013.

Under the hypothesis that the shift is statistical rather than climatological, we can use the whole series and simulate real-time forecasting. Under the alternative hypothesis that the shift is climatological, we can use only "after shift" data, i.e., 1989–2013. The latter is not sufficient for real-time forecasting simulations and cross-validation is the only applicable option. Certainly, we have no sufficient knowledge now for selection of the single correct hypothesis. Though, since the three latest winters (2010/11–2012/13) were cold, the first hypothesis looks more reasonable. Nevertheless, we performed two different sets of forecasting procedures consistent with the two different hypotheses. We performed a 30-year series of forecasts simulating the real-time procedure (30 forecasts with 25-year training periods) and a 25-year series of cross-validated three-year-leave-out forecasts (25 forecasts with 22-year training periods). The pre-forecast analysis shown in this section was performed on the 35-year series (1979–2013) mostly used in the nowadays studies.

3.1.2 Relationships between October Temperature and Wintertime Temperature: Is Prediction of Wintertime Temperature Based on Persistence Possible?

The following analysis has been performed on the series of fields from 1979-2013 (35 years), the effective sample (series) size accounting for serial correlation for most of the gridpoints is above 32 years, corresponding number of degrees of freedom is above 30 and corresponding correlation threshold value for the 5% significance level is approximately 0.35.

A routine question of any research and development (R&D) work on forecasting relates to persistence. In our case, it is as follows: "whether October temperature anomalies persist into winter?" To solve this question regarding the persistence of October temperature anomalies into the following winter, we constructed a set of correlation maps (Figures 3.1.4–3.1.6) that show the relationships between the temperature values in October and the following months. The map of the correlations between October and DJF temperature series at various gridpoints over East Asia (Figure 3.1.4) shows that we can expect some persistence only over the far eastern provinces of Russia and the central provinces of China. Over Korea, the prevailing correlations varied within 0.2–0.3.

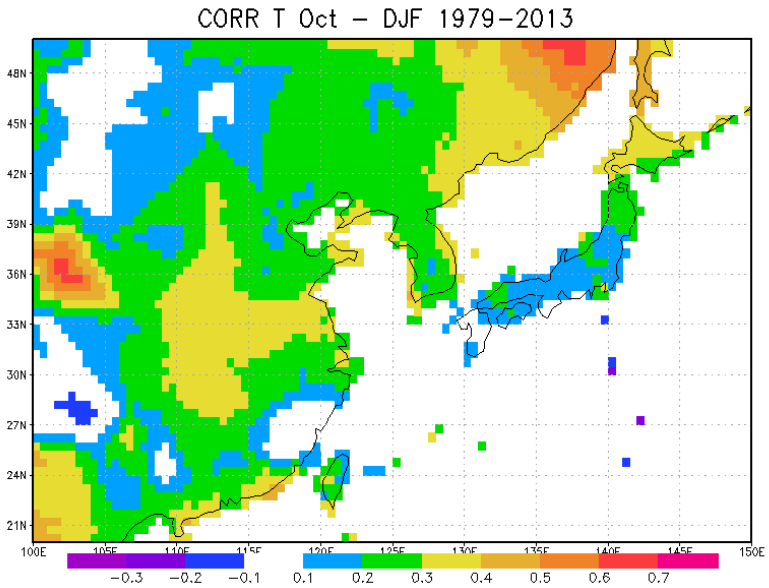

Figure 3.1.4 Correlations between October gridpoint temperature and DJF gridpoint temperature.

Whether the obtained correlations are caused by persistence or not can be revealed from the lag correlation maps between October temperature and temperature from the following months. There likely exists some persistence into November, as correlations above 0.3 over northwestern East Asia and along the coastal zone of Southern China were detected (Figure 3.1.5a). Correlations between December and October temperature series are insignificant throughout the entire East Asian region, with some local exceptions (Figure 3.1.5b). However, January temperature significantly correlates with October temperature over the coastal regions of East Asia, particularly over the West Sea and East Sea coasts and over the inner regions of Korea (Figure 3.1.5c). While enhanced "coastal" correlations are obviously a result from the persistence of West Sea and East Sea SST, the cause of the general increase of correlations in January, which is not due persistence, needs to be further studied in the future. Correlations between October and February temperature series are presumably insignificant (Figure 3.1.5d). Thus, lag correlations become insignificant in December. Such a succession of the lag correlation maps suggests no persistence into winter, thus restricting it to only November and to only some regions.

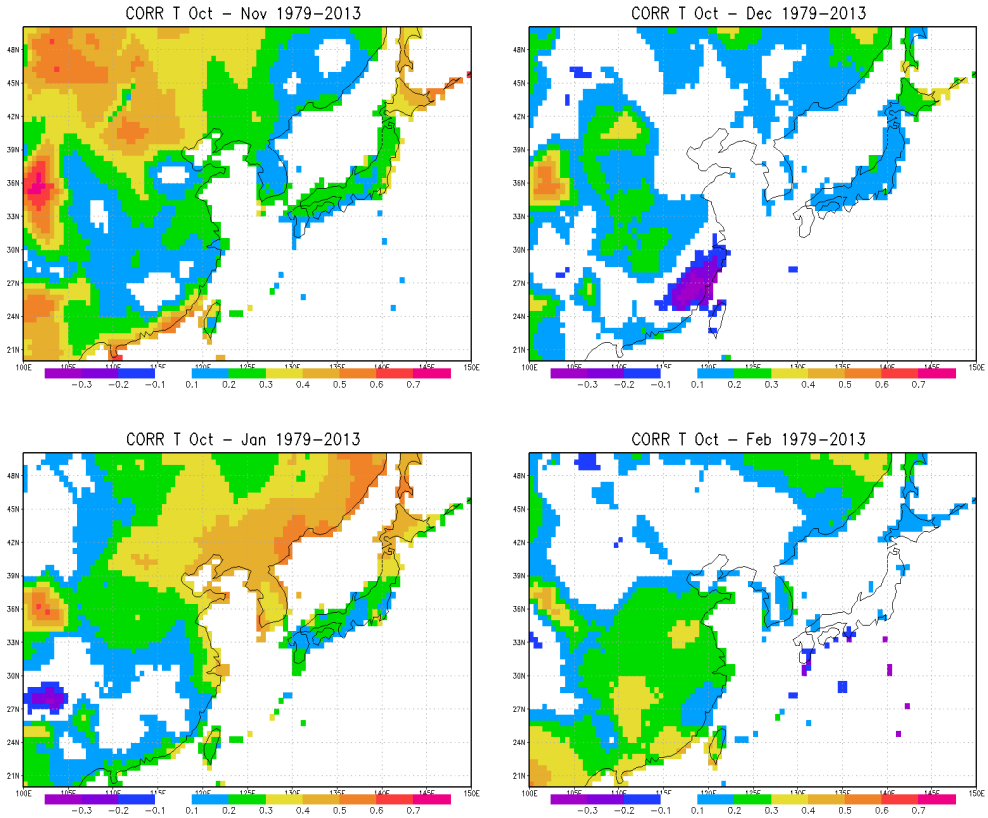

Figure 3.1.5 Correlations between October gridpoint temperature and November (a), December (b), January (c), and February (d) gridpoint temperature.

Indeed, correlations between November temperature and the following December and DJF temperature values are presumably insignificant (Figure 3.1.6), which supports the supposition on the lack of persistence. So, the statistically significant relationships between October temperature and the following winter, particularly January, temperature have to have some other explanation. For instance, it could be some kind of a bridge from the processes defining October temperature anomalies to those of January.

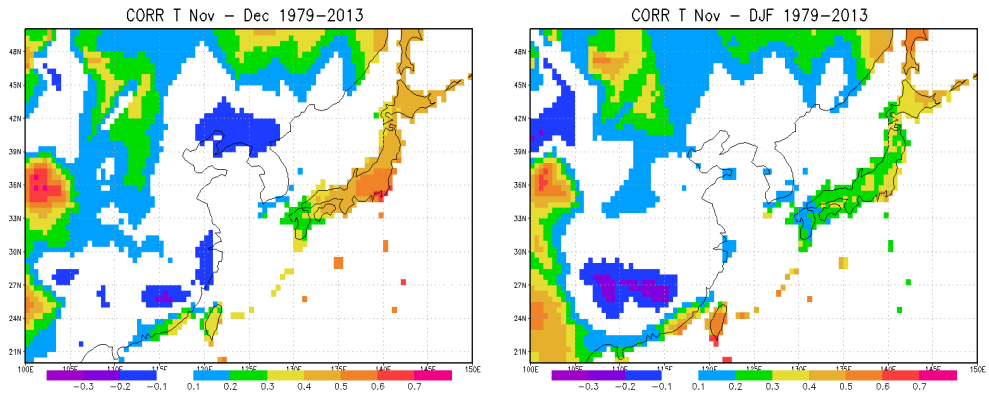

Figure 3.1.6 Correlations between November gridpoint temperature and December (a) and DJF (b) gridpoint temperature.

Correlations between the series of monthly temperature averaged over South Korea are shown in Table 3.1.1. From the table, it is clear that no method based on persistence or autoregression is reasonable for prediction of wintertime temperature over Korea. The highest achieved correlation of 0.407 is between the October and January temperature series, and this correlation only slightly exceeds the threshold of the 5% significance level; furthermore, October temperature could only explain about 16% of the January temperature variation.

The main conclusions of this analysis are as follows:

- Prediction of wintertime temperatures over Korea and East Asia as a whole by a method based on autoregression is senseless.
- Meanwhile, there may appear to be some kind of January re-emergence of the background processes/conditions influencing temperature anomalies in October. This should be investigated in a special study in the future.

Table 3.1.1 Correlation coefficients (×1000) between the series of monthly temperature averaged over South Korea for 1979–2013. Jan_{+1}–Mar_{+1} – months of the next year. Coefficients significant at the 5% level are shown in bold.

	Jan	Feb	Mar	Apr	May	Jun	Jul	Aug	Sep	Oct	Nov	Dec	Jan_{+1}	Feb_{+1}	Mar_{+1}
Jan	1000	**424**	**537**	310	63	-58	-122	-77	139	240	-107	**437**			
Feb		1000	**612**	242	197	-47	-69	3	323	270	184	**409**			
Mar			1000	**365**	121	-92	-11	-114	189	164	-81	**415**			
Apr				1000	**429**	-100	235	-36	**359**	103	27	246			
May					1000	255	103	232	**442**	**453**	75	-117			
Jun						1000	326	284	202	75	145	-194			
Jul							1000	**617**	310	255	-1	0			
Aug								1000	282	**496**	73	2			
Sep									1000	**359**	232	63	149	107	181
Oct										1000	173	79	**407**	152	221
Nov											1000	24	144	2	-31
Dec												1000	**376**	**359**	290

3.1.3 Concurrent Relationships of Wintertime Temperature with Circulation and Surface Properties

In this chapter, we analyze concurrent relationships between wintertime temperatures in South Korea and wintertime SLP, zonal flow, geopotential heights, snow cover, sea surface temperature, sea ice concentration, air temperature, and precipitation.

Maps of the correlation coefficients between DJF KST and climate variables representing the concurrent DJF climate system are shown in Figure 3.1.7. Enhancement of the polar jet and weakening of the subtropical jet, which synoptically could be treated as an anticyclonic shift in zonal wind over East Asia in the upper troposphere (Figure 3.1.7a) and lower stratosphere (Figure 3.1.7b), are favorable for a positive temperature anomaly over South Korea. This circulation anomaly corresponds to a weaker East Asian climatological (coastal) trough and, consequently, weaker advection of the cold Arctic air to East Asia, particularly Korea. This finding exactly matches the negative phase of the EAWM index of Jhun and Lee (2004).

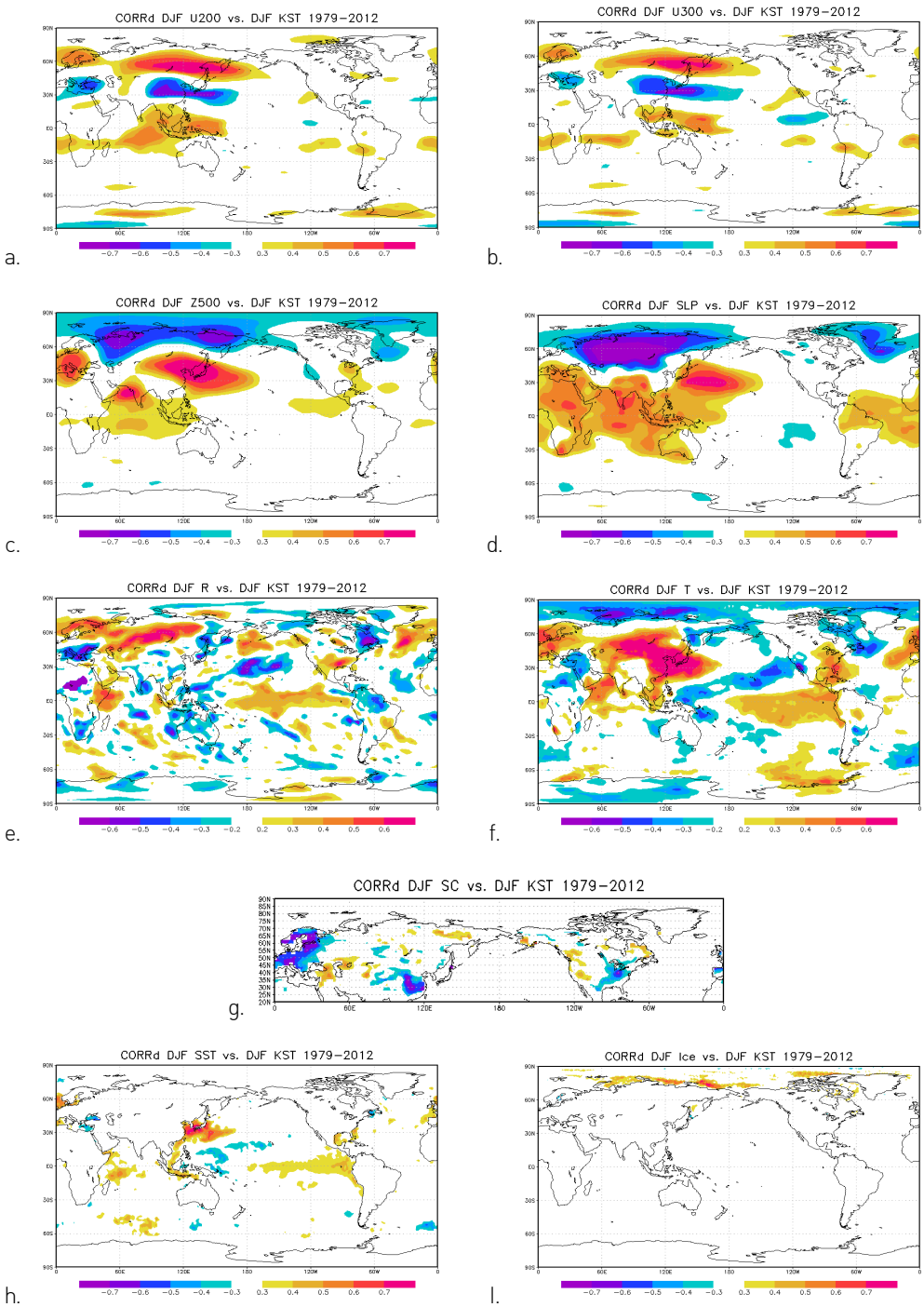

Figure 3.1.7 Maps of concurrent correlations between DJF KST and DJF U200 (a), U300 (b), Z500 (c), SLP (d), R (e), T2m (f), SC (g), SST (h), and SIC (i).

Anomalies of Z500 favorable for positive temperature anomalies over South Korea area negative anomaly over the Urals in the area of the Ural ridge, expanding eastward up to the Chukotka peninsula and a positive Z500 anomaly over East Asia, which, on the one hand, reflects a positive temperature anomaly below Z500 and which corresponds to weaker East Asia trough with corresponding changes in advection and planetary wave generation (Fig. 3.1.7c). The SLP anomalies favorable for positive temperature anomalies over Korea (Figure 3.1.7d) are a vast area of the negative anomalies spanning the whole Northern Eurasia northward from the central latitude of the SH, that is, some weakening and shift of the Siberian high southward. And a belt of positive SLP anomalies surrounding Southern Eurasia with the strongest correlations spanning subtropical and lower extratropical western North Pacific. In general, regarding to circulation, favorable for a DJF KST positive anomaly is enhancement of (at least) tropospheric and lower stratospheric zonal circulation, enhancement of the zonal flow in the latitudinal belt 40°N-70°N (approximately) which corresponds to the positive correlation (0.4) with the DJF AO.

Consistent with circulation anomalies are anomalies in precipitation (Figure 3.1.7e) and temperature (Figure 3.1.7f). The most prominent feature is a wide strip of positive precipitation anomalies in northern Eurasia from Scandinavia through East Siberia, which denotes the prevailing routes of cyclones and associated frontal systems that separate the (comparatively) warm southern Siberia and East Asia from the cold Arctic air concentrated over the marginal Arctic seas. In combination with a negative snow cover anomaly over Europe (Figure 3.1.7g), i.e., prevailing temperature above the melting point, it indicates a northward shift in the North Atlantic stormtracks. Meanwhile, a positive precipitation anomaly in the equatorial Pacific in combination with a positive SST anomaly (Fig. 3.1.7e) indicates a tendency towards El-Nino (It should be noted that precipitation anomalies are analyzed because they essentially improve understanding of the relationships between atmospheric and surface variables rather than they are considered as a possible predictor). South Korea is located on a peninsula so, expectedly, its temperature strongly correlates with SST of surrounding seas (Figure 3.1.7e); it should also be noted a close consistency between the SLP (Figure 3.1.7d) and SST (Figure 3.1.7h) anomalies in the subtropical western North Pacific.

Positive correlations with SIC (Figure 3.1.7i) are due to the high persistence of SIC in general and also due to the tendency for higher October SIC in the eastern Arctic to precede winters with positive KST anomalies (as will be shown and discussed in the next section). It's interesting to note the dual nature of the impacts on DJF KST revealed in Figure 3.1.7. On the one hand, over northern Eurasia, the relationships of DJF KST and AOI with other variables closely resemble each other. On the other hand, over the equatorial and even mid-latitude Pacific, the relationships of DJF KST with local variables are inverted to the corresponding relationships of the DJF AOI. This may be the reason why the positive correlation between DJF KST and AOI is not strong, 0.40.

The main conclusions of this analysis are as follows:
Wintertime temperature over Korea is significantly concurrently related to other wintertime climate variables.

- In general, enhancement of the zonal circulation over the Northern Hemisphere extratropics is favorable for a positive temperature anomaly over Korea.
- These findings have implications for predictions, namely, if direct relationships between October variables and DJF temperatures appear too weak to provide reasonable skill for predictions, the concurrent wintertime climate variables may be able to play a role as interim predictors.

3.1.4 Lag Relationships of Wintertime Temperature with October Circulation and Surface Properties

Table 3.1.2 shows that positive Korean Peninsula temperature anomalies tend to be preceded by the negative phase of the October Taymyr circulation anomaly described in Kryjov (2015), which is a significant predictor of the DJF AO positive phase. Meanwhile, the October AO correlates insignificantly with the Taymyr Circulation Index (TCI), the DJF KPTs, and the AO.

Table 3.1.2 Correlation coefficients between the Korean Peninsula DJF temperature (KPT) and precipitation (KPR) and the October Taymyr Circulation Index (TCI), AO Index (AOI), and DJF AO Index (AOI) for 1979–2013. Coefficients shown in bold are significant at the 5% level.

	KPR	TCI	AOI	AOI
KPT	0.214	**-0.365**	-0.028	**0.453**
KPR		0.051	-0.175	0.068
TCI			-0.281	**-0.621**
AOI				0.253

The lag correlations between DJF KST and October variables among which the predictors for wintertime KST could be selected are presented in Figure 3.1.8. Correlation maps shown in Figures 3.1.8a–3.1.8d reveal not strong but statistically significant relationships between DJF KST and October cyclonic circulation over the Taymyr Peninsula, quasi-barotropically spanning, at least, the upper troposphere from 500 hPa through 200 hPa in the lower stratosphere. This pattern closely resembles a negative phase of the Taymyr circulation anomaly (TCA) described in Kryjov (2015), it tends to precede a positive phase of the DJF AO and confirms the values in Table 3.1.2. The associated advection of warm air to East Asia enhances the positive geopotential height anomalies (a weakening of the East Asian trough), which is somewhat apparent in Figures 3.1.8a–3.1.8d; however, this relationship is readily apparent in Figures 3.1.7a–3.1.7c (discussed in the previous section). In general, enhancement of the tropospheric–lower stratospheric zonal flow in the latitudinal belt at 50°N–80°N during October is favorable for positive DJF KST anomalies.

a.

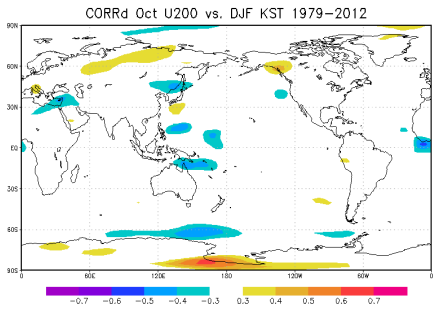

b.

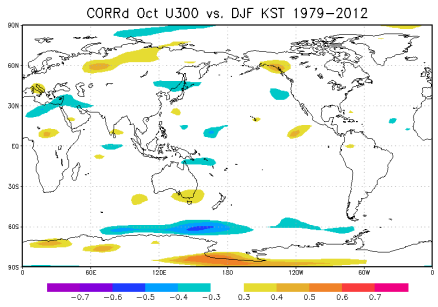

c.

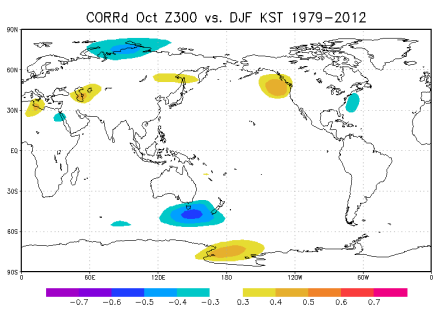

d.

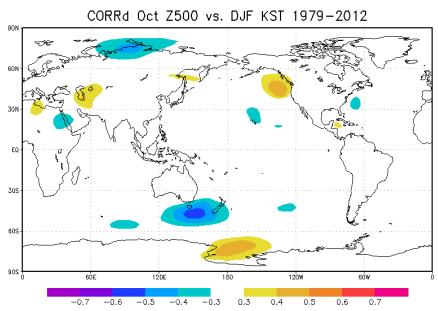

e.

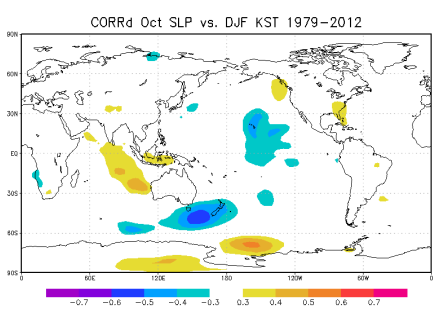

Figure 3.1.8 Continuation on the next page.

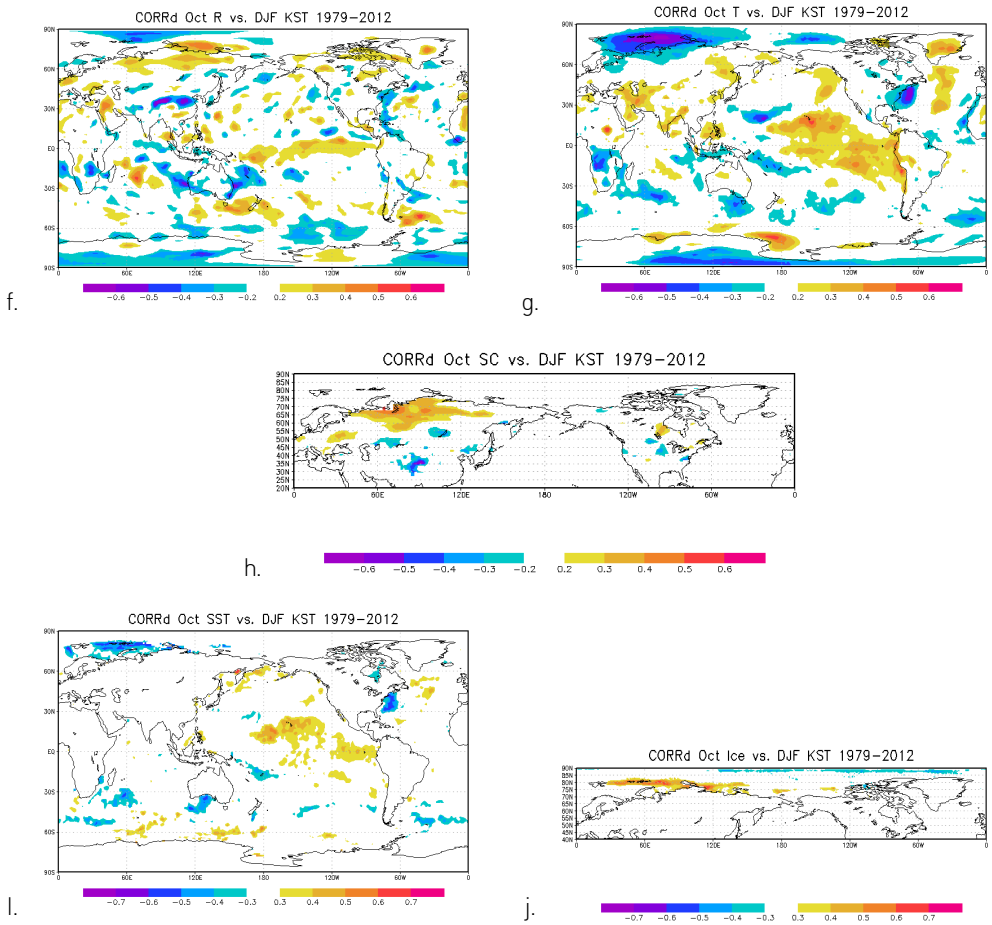

Figure 3.1.8(Continuation) Maps of lag correlations between DJF KST and October U200 (a), U300 (b), Z300 (c), Z500 (d), SLP (e), R (f), T2m (g), SC (h), SST (i), SIC (j).

Lag correlations of DJF KST with October SLP (Fig. 3.1.8e) indicate a tendency of a positive DJF KST anomaly to be preceded by an October (developing) El-Nino, which is also supported by positive correlations of DJF KST with equatorial Pacific precipitation (Fig. 3.1.8f) and SST (Fig. 3.1.8i). Correlations between DJF KST and October SLP over the Taymyr peninsula and adjusted seas is negative similarly to Z500 and Z300, however, much weaker (-0.2 – -0.3) which could be explained with the correction/adjustment errors since the Taymyr peninsula is a mountain region with heights exceeding 1000 m. Correlations between DJF KST and October precipitation (Fig. 3.1.8f), snow cover (Fig. 3.1.8h), SIC (Fig. 3.1.8j) in the northern

Eurasia and SST in the Barents and Kara seas (Fig. 3.1.8i) are consistent with those between DJF KST and October circulation (Figs. 3.1.8a-3.1.8e). The correlations indicate that prior to winters of the positive KST anomaly, there is a tendency to enhanced precipitation over the northern (sub-polar) Asia which likely indicates intensification of the frontal zone, with corresponding positive anomaly of the snow cover, negative SST, T2m and positive SIC anomalies in the Barents and Kara seas.

It is interesting to note that the maps shown in Fig. 3.1.8 demonstrate high consistency between the possible October predictors of DJF KST. And, logically, it is just circulation that affect and adjust other variable fields, with effect from the surface properties being exposed rather as a positive feedback than an one way impact, correlations of KST with circulation variables are rather weak, meanwhile correlations with the surface properties are quite high with absolute values of up to 0.5 - 0.6. The possible explanation may reside in larger noisiness of the circulation variable series as compared with surface properties because the latter reflect accumulated impact from circulation – SST and SIC anomalies reflect accumulated impact of mainly surface winds; and snow cover anomalies via precipitation and temperature accumulate impacts of pressure/geopotential field anomalies.

The main conclusions of this analysis are as follows:

- These findings have implications for predictions in that the DJF temperature anomalies over Korea are preceded by regional anomalies of October variables, with the highest linear relationships (correlations (absolute values) of up to 0.5–0.6) involving October snow cover in northern Eurasia and SSTs and SIC in the Barents and Kara seas.

The mostly generalized feature of the DJF circulation pattern favorable for the positive temperature anomalies over Korea is prevailing of zonal circulation in troposphere and, at least, lower stratosphere. It makes sense to test the AO as a “corresponding” pattern. That is to test prediction of East Asia temperature using predictors selected for prediction of the wintertime AO.

3.2 Prediction of the Wintertime Arctic Oscillation Based on Autumn Circulation: Prediction of Wintertime East Asia Temperature with the Use of the Arctic Oscillation-Selected Predictors

3.2.1 Introduction

The Arctic Oscillation (AO) recognized by Thompson and Wallace (1998, 2000) is a dominant mode of the wintertime atmospheric variability of the Northern Hemisphere strongly affecting weather and climate of the vast regions of North America and Eurasia. On the seasonal time scale it has an equivalent-barotropic structure from the surface through the middle stratosphere at least.

Reliable prediction of the wintertime AOI well in advance, with one month lead at least, is a priority for extratropical seasonal prediction (Smith et al., 2014). So, development of a method of prediction of the wintertime AO is a challenge itself. It is the first goal of the study. The second goal is KST prediction. Although correlation between the DJF AOI and KST is not high, about 0.40, October predictors, selected for the DJF AOI, may open a way for prediction of KST strongly related to wintertime circulation. And the third goal of the study presented in this section is a test of the prediction method described in Section 2 and Appendices. It is reasonable to test the newly developed methods on some global-scale variables with known prediction skill. So that, we have started prediction analysis with the wintertime AO. A shortened version of this section shaped as a paper was published at International Journal of Climatology (Kryjov and Min, 2016).

Zero lead numerical model predictions of the December-February (DJF) mean AOI are quite skillful (Kang et al., 2014). However, only few seasonal climate prediction models are able to predict the DJF AOI with a one month lead. A CFSv2 ensemble prediction is reported to provide above 20% of explained variance of the DJF AOI on a 28-year series (Riddle et al., 2013). A GloSea5 model achieves correlation of 0.63 on a 14-year series (Scaife et al., 2014, MacLachlan et al., 2014). A climate model of Pusan National University predicts the DJF AOI with correlation 0.60 on a 30-year series (Ahn and Kim, 2013; Sun and Ahn, 2014). That is, one month lead predictions of the most successful state-of-the-art models are able to explain up

to 35-40% of the DJF AOI variance. Correlation coefficient between the APCC MME predicted DJF AOI and observations is 0.26 (hindcasts from 1983-2007), with individual model historical forecasts correlating with observations with coefficients ranging from -0.12 to 0.37 (Shin, APCC Report-2014).

Correlation between the DJF (Dec) AOI and October AOI is 0.17 (0.12), so that prediction of the wintertime AOI based on the October AOI is senseless. Instead, a number of October drivers of the wintertime AO have been found (e.g., Cohen et al., 2007; Garfinkel et al., 2010; Folland et al., 2012; Scaife et al., 2014). Particularly, the phases of solar cycle, QBO, El-Nino/Southern oscillation (ENSO), and North Atlantic SST tripole; anomalies of snow cover in Eurasia and the Kara Sea SIC and SST. They are mainly used in the forecast supporting expert assessments rather than in the formalized forecasting procedures, e.g., statistical models (at least, according to publications of the recent decade). A most known (unless a single) exclusion is snow cover in Eurasia.

A one month lead statistical prediction method for the DJF AOI has been developed by Cohen and coauthors (e.g., Cohen et al., 2007; Cohen and Fletcher, 2007) who have demonstrated strong relationships between the DJF AOI and an October anomaly of Siberian snow extent represented numerically by the Snow Cover Extent Index (SCE). The relationships were weakening in the 2000s and Cohen and Jones (2011) have suggested a new index, the Snow Advance Index (SAI) characterizing an October rate of snow cover extent increase. However, Peings et al. (2013) show that the relationships of the wintertime AO with both SCE and SAI are not stationary and were statistically significant only in the late 20^{th} and early 21^{st} Centuries.

Another October precursor of the DJF AO, a geopotential height anomaly over the Taymyr Peninsula and the Laptev Sea (Taymyr circulation anomaly, TCA), has been suggested by Kryjov (2015). The author documents that the October TCA affects the DJF AO phase by the tropospheric temperature advection of inverse signs to the central Arctic and to the East Asia, with the cyclonic (anticyclonic) TCA tending to precede winters of the positive (negative) AO polarity. His study shows that both SIE and SAI are closely related to the TCA via Eurasian precipitation anomalies excited by those of circulation. A correlation between the wintertime AOI and an October index associated with the TCA, the Taymyr circulation index (TCI), is -0.58, with

the relationship being stationary throughout the whole analyzed period, 1958-2012.

The strong correlations and stationarity of the established relationships allow one to consider the October TCI as a possible predictor of the DJF AOI. However, independent assessments of the TCI as a predictor are impossible for 1959–2013, which represents the period in which these relationships were established (e.g., Folland et al., 2012). Thus, to provide independent data for forecast assessments, we had to use simulation forecast procedures for the real-time forecasts, with the predictor for each forecast being constructed independently rather than predefined.

3.2.2 Data and Methods

The study is mainly based on the data from the National Centers for Environmental Prediction–National Center for Atmospheric Research (NCEP-NCAR) Reanalysis (Kalnay et al., 1996) available at the International Research Institute for Climate and Society/Lamont-Doherty Earth Observatory web site (ingrid.ldeo.columbia.edu).

The monthly AOIs, are estimated for 56 years (1958-2013) following the definition of Thompson and Wallace (2000) and methodology of Climate Prediction Center (CPC) but with a basis period 1958-1983. The mean wintertime AOI, the predictand, is estimated for 55 winters (1959–2013, hereafter winter years as of January) as an average of three monthly (December, January, February) indices and normalized with the reference period 1959-1983. The obtained AOI closely covariates with that of CPC, with the correlation between the indices being 0.99 for the 55-year series. However, a difference in means between the estimated index and that of CPC is 0.69 for the same 55-year period.

Predictor series are derived from October (1958–2012) fields of geopotential height of 500 hPa surface (Z500) northward of 20°N. We use sea ice concentration (SIC) and sea surface temperature (SST) from the Hadley Centre Sea Ice and Sea Surface Temperature data set (HadISST) detailed by Rayner et al. (2003) and available at www.metoffice.gov.uk/hadobs/hadisst. Precipitation and snow cover data are those of 20th Century Reanalysis (Whitaker et al., 2004; Compo et al., 2006; Compo et al., 2011) available at the Earth System Research Laboratory site (www.esrl.noaa.gov).

We estimate by means of regression and verify 30 forecasts of the AOI for the winters of 1984-2013, with the training being performed on the 25-year series preceding a forecast year. Following requirements of independency, we use no predefined predictor, particularly we do not use the October TCI of K15 which highly correlates with the DJF AOI. Instead, for each forecast we estimate a unique predictor by projecting the whole Z500 field north of 20°N onto a correlation map between the DJF AOI and October Z500 series at the grid-points, with grid-point weights being provided by the correlation map. This approach is similar to that of Lee et al. (2013). However, we do not predefine any thresholds for grid-point correlations.

The prediction procedure consists of five steps. On the first step, we compute a correlation map of October Z500 and the DJF AOI using the data from the training period (25 years). On the second step, we construct a predictor, a 25-year series of a "Circulation Index" computed as a projection of October Z500 anomaly fields on the correlation map. On the third step, we derive a regression equation based on the 25-year training period. The fourth is estimation of the 26^{th} year predictor by projecting of the October Z500 field from the 26^{th} year onto the correlation map. The fifth step is estimation of the forecast value of the DJF AOI using the 26^{th} year value of the predictor.

Verification assessments are based on retrospective predictions, with prediction procedures exactly reproducing those of real-time forecasts. Performance of the forecasts is assessed by a Mean Square Skill Score (MSSS), with reference forecasts being climatological ones (Murphy, 1988), and a temporal unadjusted correlation (congruence) coefficient (TCC) also known as an anomaly correlation coefficient.

Based on the available data with an intent to have a longer time interval for the verification assessments, we appoint a 25-year reference period (1959-1983) and estimate the DJF AOI as departures from its climatology (mean value) from this period. However, because of prevailing of the positive AOI departures from the reference period climatology in both prediction and observation series, the verification assessments may appear overestimated. Another strategy is to verify predictions of the AOI as departures from the climatologies of the sliding training periods. We have performed both and show results from both. These two verification strategies correspond to the cases III (single-valued external climatology) and IV

(multiple-valued external climatology) of Murphy (1988).

3.2.3 Results

3.2.3.1 Predictors

A summary of correlation maps underlying the forecasts is provided in Figure 3.2.1. Shown are the numbers of forecasts out of 30 for which the absolute values of the training period correlation coefficients exceed 0.4 (approximately the 5% significance level). In close consistency with Kryjov (2015), the largest number of years with significant (negative) correlations is over the TCA area. Corresponding negative anomalies of Z500 in conjunction with the positive Z500 anomalies in the middle latitudes intensify zonal circulation in the latitudinal belt 50°N-70°N over Eurasia, prevent an advection of the warm Atlantic air to the central Arctic and provide the warm south-western advection to East Asia, which results in lower geopotential over the central Arctic and weakening of the East Asia trough, with both results being favorable for the enhancement of the circumpolar vortex (Holton, 2004) and, consequently, the positive AOI polarity.

The correlation coefficients between the series of estimated predictors with the inverted October TCI from the corresponding 26-year periods ended on the years of forecasts indicated in the abscissa axis are shown in Figure 3.2.2. All the correlation coefficients are significant at the 95% confidence level at least. For the forecast years after 1988, with 26-year long predictor series starting after 1963, all the inverted correlation coefficients are within 0.74 – 0.93 which is well above the 99% confidence level threshold. For the first six forecasts (1984 – 1988) correlations between the predictors and the corresponding TCI series are lower, 0.43 - 0.60. This difference may result from either unstable relationships probably caused by climate shift of the late 1970s or poor tropospheric data of the 1950s-1960s, or both causes. For 30 training periods, normalized regression (correlation) coefficients between 30 series of the predictor and the DJF AOI vary within the range 0.64 to 0.78, with the average value being 0.72 and all the coefficients being significant at the 99% confidence level. Values of the Darbin-Watson statistic indicate no correlation in residuals.

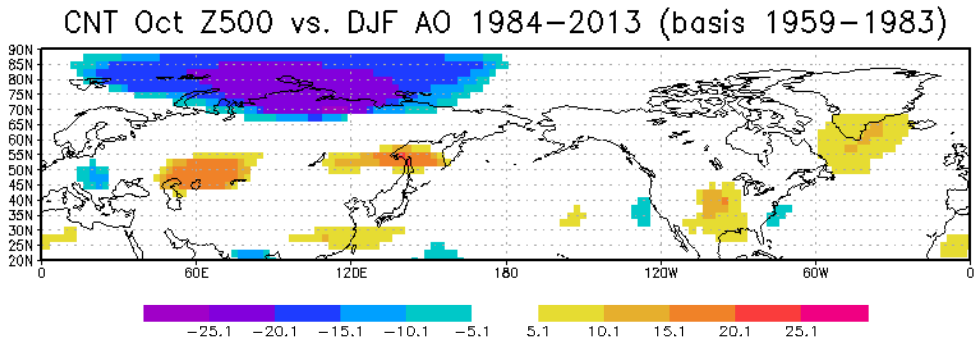

Figure 3.2.1 The number of forecasts (out of 30) with an absolute value of the correlation coefficient between the DJF AOI and October Z500 exceeding 0.4 (shading); positive (negative) values correspond to positive (negative) correlation coefficients; the numbers with absolute value exceeding 5 are significant at the 99% confidence level in the test based on Binomial probability distribution.

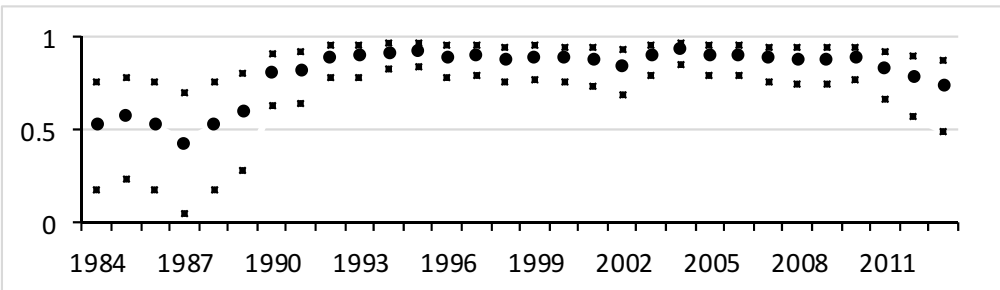

Figure 3.2.2 Correlation coefficients (circles) between the constructed predictors and the (inverted) TCI for the sliding 26-year windows covering a training period and a forecast year. The 95% confidence intervals are shown as squares. The correlation coefficients are plotted in the forecast year, e.g., the correlation coefficient plotted in 1984 represents the 25-year training period 1959–1983 and the forecast year 1984.

3.2.3.2 Verification assessments

The skill of the obtained forecasts is quite high. For the verification strategy with the AOI values defined as departures from the climatologies estimated over the sliding training periods, the TCC is 0.61 and MSSS is 0.37. When the AOI values are defined as departures from the fixed 1959-1983 climatology, both TCC and MSSS increase up to 0.66 and 0.43, respectively. All the obtained scores are above zero at the confidence level well exceeding 95% in bootstrap 1000 Monte Carlo trails (Wilks, 1995).

Time series of the predicted and observed DJF AOI (departures from the sliding climatologies) are shown in Figure 3.2.3. With exclusions of two extreme AOI years, the observed AOI values lie within the 95% confidence intervals of the predictions. For the years of extremes, 1989 and 2010, the sign of the AOI is predicted correctly, however, the absolute value of the index is essentially underestimated. On the one hand, an underestimation of extremes is an inherent feature of regression models which may perform improperly beyond a range of variability of climate variables during the training period. On the other hand, the underestimation of extremes shows the limits of our method which is confined to only extratropical tropospheric circulation as a predictor. The cyclonic TCA of October 1988 and the following extremely high AOI winter of 1989 occurred on the background of La-Nina, a westerly phase of the Quasi Biennial Oscillation (QBO) and a solar maximum in its 11-year cycle, that is, on the background favorable for the wintertime strong undisturbed circumpolar vortex and the corresponding positive AO polarity (Camp and Tung, 2007; Kryjov and Park, 2007). Inversely, the extremely low AOI winter of 2010 and preceding October anticyclonic TCA occurred on the background of El-Nino, an easterly phase of the QBO and a solar minimum resulted in the strongly disturbed weak circumpolar vortex (e.g., Wang and Chen, 2010) and the corresponding negative AO polarity.

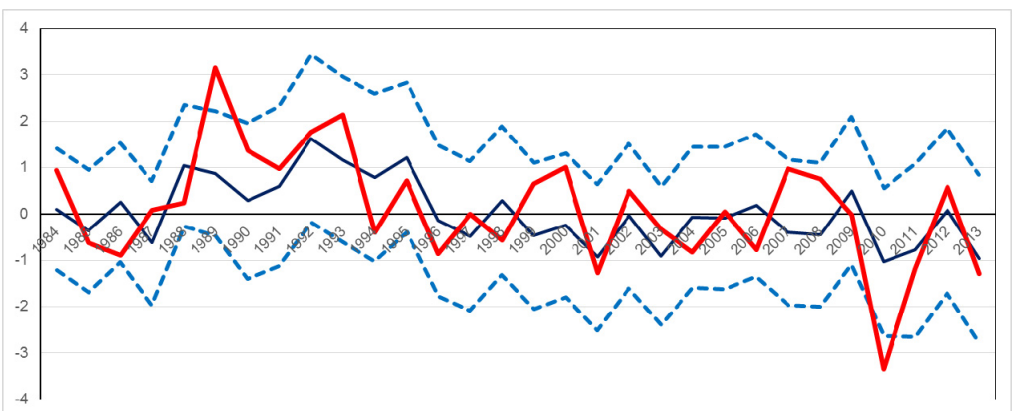

Figure 3.2.3 Time series of the DJF observed (red) and predicted (blue) AOI. Dashed lines denote the 95% confidence intervals of the predicted AOI.

Meanwhile, in general, the ratio between the standard deviations of the independent forecasts and observations of the DJF AOI exceed 0.56 for both options of the AOI reference period definitions. It is worth noting that increase of the training period up to 30 years (with corresponding decrease of the verification period down to 25 years) expectedly increases shown above values of TCC and MSSS by 0.02-0.04.

The wintertime AO strongly affects concurrent temperature over the northern extratropics (Thompson and Wallace, 2000). To confirm the skill of the DJF AOI forecasts we have predicted 30 DJF temperature fields with the use of the corresponding October predictors constructed for the DJF AOI forecasts. Verification assessment of these temperature forecasts reveals that the patterns of the TCC values significant at the 95% confidence level (Figure 3.2.4) closely resemble those associated with the strong impact of the DJF AO on concurrent temperature (e.g., Figure 2a of Cohen and Fletcher, 2007), that is, the Northern Eurasia, eastern Mediterranean, Greenland and the Labrador Peninsula, Eastern North America. This provides support to the results of the verification assessments of the DJF AOI forecasts and expands an area of applications of the method. Particularly for East Asia temperature forecasts are skillful for Manchuria and not skillful for south-eastern China. For South Korea TCC is within 0.3-0.5 with exclusion of the eastern coast.

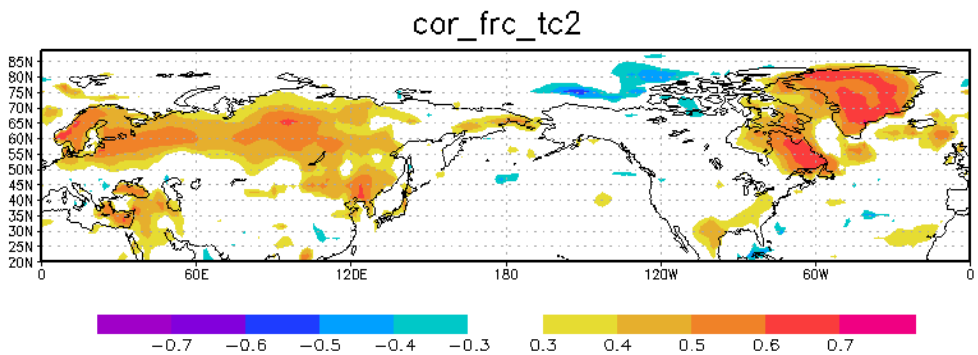

Figure 3.2.4 The TCC between the observed and predicted DJF temperature anomalies for the winters 1984–2013.

3.2.4 Discussion

The selected Z500-based predictors indicate anomalies closely resembling the TCA of K15. Physically plausible mechanisms of the October TCA impact on the DJF AO reside in weakening (enhancement) of the East Asia trough and associated planetary waves with wave numbers 1 and 2 and decreasing (increasing) of geopotential in the polar area in Octobers preceding the winters of the positive (negative) AO polarity.

Summarizing results from the previous studies on the autumn impacts on the wintertime North Atlantic climate anomalies and the AO (e.g., Cohen et al., 2007; Garfinkel et al., 2010; Folland et al., 2012; Scaife et al., 2014), one may draw up a list of autumn precursors of the wintertime AOI. Particularly, the phases of solar cycle, QBO, El-Nino/Southern oscillation (ENSO), and North Atlantic SST tripole; anomalies of snow cover in Eurasia and the Kara Sea SIC and SST.

Among these precursors, we focus only on those directly linked to the Z500 anomalies over the Taymyr Peninsula. We analyze them, along with SLP and precipitation, by means of 30-year independent predictions, with the prediction procedure being similar to that based on Z500 and explained above. The numbers of years with correlations exceeding 0.4 are shown in Figure 3.2.5. Prevailing October SLP anomalies (Figure 3.2.5a) preceding winters of the positive AO polarity are consistent with the prevailing anomalies of Z500 associated with the TCA. Consistent with SLP are the prevailing precipitation anomalies (Figure 3.2.5b). Those comprise a belt of enhanced precipitation in the northern North Eurasia (north of 60°N) and a weaker pronounced belt of negative precipitation anomalies over the southern Siberia (40°N-50°N). Prevailing October anomalies of snow cover (Figure 3.2.5c) are closely consistent with those of precipitation, that is, positive snow cover anomalies in the northern East Siberia and negative anomalies in the southern Siberia. Spatial distribution of the anomalies of these three variables are closely consistent with each other and all are consistent with the anomalies of Z500 closely resembling the TCA.

The maps for SIC and SST show close consistency between the SIC and SST anomalies in the Kara Sea (Figures 3.2.5d and 3.2.5e) and consistency of both with

the SLP anomaly over the Taymyr Peninsula indicated in Figure 3.2.5a. The anomalous north-westerlies in the western periphery of the negative SLP anomaly cause the drift of sea ice and colder surface water into the Kara Sea. Spatial consistency between the Z500-based predictors and those based on other variables, especially SLP, precipitation and snow-cover, is supported by high temporal covariability of their time series, with the correlations of the Z500-based predictors with those SLP-, precipitation- and snow cover-based being 0.80 - 0.95, 0.70 – 90 and 0.60 – 0.90, correspondingly. Although the skill of the DJF AOI forecasts based on these variables is lower than that based on Z500, all them (with reasonable exception of precipitation shown in illustration purposes) could be considered as potential predictors for the wintertime zonal circulation intensity.

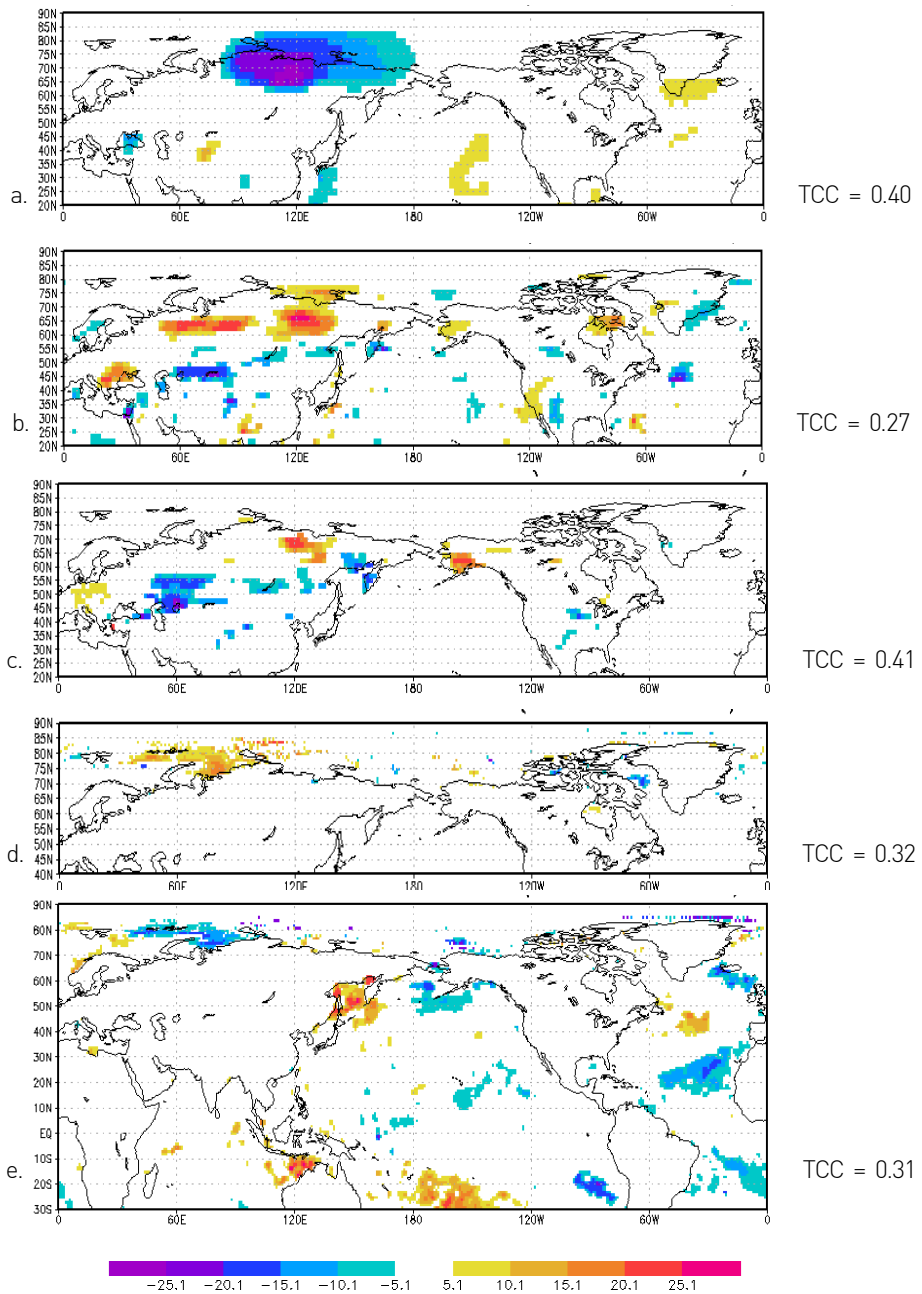

Figure 3.2.5 The number of forecasts (out of 30) with an absolute value of the correlation coefficient between the DJF AOI and October SLP (a), precipitation (b), snow cover (c), SIC (d), SST (e) exceeding 0.4 (shading); positive (negative) values correspond to positive (negative) correlation coefficients; the numbers with absolute value exceeding five are significant at the 99% confidence level in the test based on Binomial probability distribution. The TCC values corresponding to the AO predictions based on the shown predictors are printed at the right side of the figures.

That is, the certain polarity of the DJF AO is preceded by the certain status of the northern extratropical climate system in October. Particularly, winters of the positive AO polarity tend to be preceded by the negative October TCA, which prevents advection of the warm air to the central Arctic and cold air to the East Asia and, consequently, leads to decrease of geopotential in the polar area and weakening of the planetary waves with wave numbers 1 and 2. Associated anomalies are those of SLP because the TCA barotropically spans the whole troposphere from the surface; an enhancement of the precipitation belt over the northern Eurasia with the positive snow cover anomaly caused by this enhanced precipitation and corresponding weakening of the precipitation belt over the southern Siberia with the negative snow cover anomaly caused by this weakening. In terms of climatological fronts (Serreze and Barry, 2005), it could be described as enhancement of the Arctic front and weakening of the Polar front. Also, preceding the positive AOI winters the Kara Sea negative SST and positive SIC October anomalies are linked to the TCA as well, they are caused by anomalous north-western advection into the Kara Sea with corresponding cooling of the surface water and increasing of concentration of drifting ice. Prior to winters of the negative AO polarity the signs of anomalies are inverted.

3.2.5 Conclusion

The carried out study has provided significant support to the strong relationships between the DJF AO and October circulation, with the October Z500-based predictor pattern closely resembling the TCA and predictor series strongly correlating with the TCI of Kryjov (2015). The October anomalies of the Eurasian snow cover, Kara Sea SST and SIC preceding certain polarity of the DJF AO are closely related to the circulation and are rather the results from than the causes of the October circulation anomalies. It should also be noted that potential predictors of the wintertime AO resemble those of the wintertime KST (Fig. 3.1.8).

A simple regression method for prediction of the DJF AO based on October circulation with flexible construction of the predictors tested on independent data has shown its efficiency. Verification assessments performed on the series of 30 forecasts of the DJF AOI reveal the TCC between the predicted and observed DJF

AOI being 0.61-0.66 and MSSS being 0.37-0.43. Prediction of the CPC's AOI is on the same skill level, TCC=0.60, MSSS=0.36.

This skill is comparable with the skill of the most successful numerical model forecasts. It implies that the method may be applied for prediction of the wintertime AO both solely and in combination with numerical seasonal models of similar skill. The second option is preferable because the suggested statistical prediction method and seasonal model forecasts are based on the different sources of predictability, particularly, our statistical forecasts are based on the October extratropical circulation anomalies while seasonal model predictions are mainly governed by tropical SST anomalies.

To conclude the section, it should be noted that the obtained results completely match expectations and fulfil the purposes of the carried out study:

1. The developed physical-empirical model for one month lead prediction of the wintertime AO yields the skill of prediction at the level of two best models.
2. Application of the AO-tuned model to one month lead prediction of the wintertime temperature anomaly yields the high skill of predictions for northern East Asia (TCC = 0.4 – 0.7) and South Korea (TCC = 0.3 - 0.5) in accordance with the wintertime AO impact on concurrent temperature.
3. The basic statistical tool for the particular implementations in physical-empirical models has been developed and tested in real-time-forecast-simulation mode for prediction of the wintertime AO.

3.3 Prediction of East Asia Wintertime Temperature for 1984–2013: Simulating Real-Time Mode with the Use of the Whole Series (1959–2013)

As a necessary note, the results presented in Sections 3.3, 3.4, and 3.5 cannot be considered to have been obtained from independent data. We have tested a number of variables as potential predictors for each target variable and selected the best one or two of them by means of stepwise multiple regression.

3.3.1 Prediction of East Asia Temperature Fields

East Asia covers a large area, and its wintertime temperature features a strong spatial variability, with DJF EAT EOF1 explaining only 53% of the total variance of DJF EAT. So that, similarly to Lee et al. (2013a) we decomposed DJF EAT into EOFs, predicted each EOF separately and then composited EAT fields associated with each predicted EOF. Further details about this method of prediction are described in Appendix 1.

Decomposition of the DJF EAT into EOFs reveals that above 80% (53%, 21%, 10%) of DJF EAT total variability is explained by three leading EOFs well separated from each other according to the rule of thumb (Wilks, 1995). So that, we truncate the decomposition to these three EOFs. It should be noted that as it is explained in Appendix 1 the units in our approach are kept in EOFs and the PCs are standardizes and unitless.

Prediction is performed in retrospective simulation of “real-time” forecast procedures. We performed 30 predictions using sliding 26 year intervals, with the first 25 years being a training period and the 26^{th} year being a forecast one.

3.3.1.1 Prediction of East Asia temperature EOF1

EOF1 of East Asia DJF temperature is shown in Fig. 3.3.1 as a correlation map between temperature fields and PC1. It is a dome with correlations well above 0.7 over central-eastern China surrounded by wings of decreasing correlations. Correlations between the PC1 and Korea gridpoint temperature series vary within 0.5 – 0.7. The PC1 time series is shown in Fig. 3.3.2. It features a well pronounced interannual variability with exception of the 1990s. In the decadal scale view, it resembles a wave with a trough in the 1970s and a ridge in the 1990s.

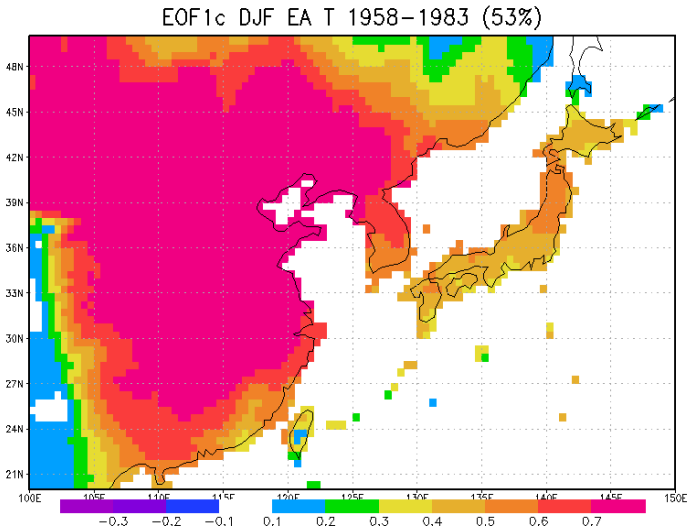

Figure 3.3.1 The DJF EAT EOF1 shown as a correlation map between temperature fields and PC1.

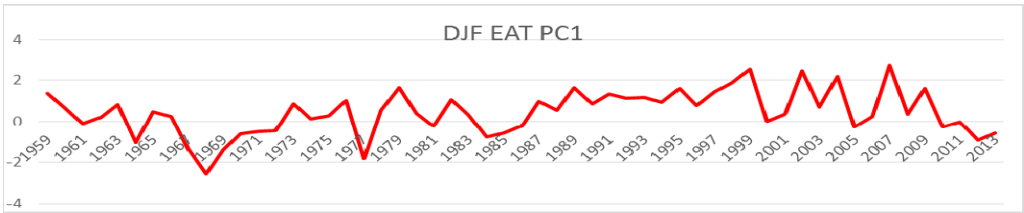

Figure 3.3.2 Time series of the PC1 for the DJF EAT.

We have tested the fields of Z500, Z300, SLP, SC, SIC, SST as potential predictors. Two predictors based on the SC and SST fields have been selected for DJF EAT PC1. Figure 3.3.3 shows the number of forecasts (out of 30) for which DJF EAT PC1 significantly correlates with the SC and SST series. First, we should take note of the obvious similarity between the numbers of significant correlations and the correlation maps shown in Figure 3.1.8 in Section 3.1, which obviously support each other. Meanwhile, as shown in the map in Figure 3.3.3a, the main DJF EAT PC1 predictability is associated with the positive correlations (larger SC) over northern North Eurasia rather than the negative correlations in the latitudinal belt at 40°N–55°N that were expected from the literature (Watanabe and Nitta, 1999; Jhun and Lee, 2004; Cohen et al., 2007 and references therein) but not revealed here. Enlarged areas of snow cover over northern North Eurasia were associated with larger

precipitation anomalies, which, in turn, are associated with shifted northward routes for cyclones and intensification of the climatological frontal zone, that is, with enhancement of the zonal circulation over northern North Eurasia as marked in Figure 3.1.8.

Interpretation of the map shown in Figure 3.3.3b (SST) is not so obvious. The main areas of the frequent occurrence of significant correlations included the northwestern Pacific and northwestern Atlantic. Accounting for the SST persistence, the northwestern Pacific area marks the preceding strong positive correlation area shown in Figure 3.1.8, which was indicative of warm westerly and northerly anomalies in the surface currents. This may also affect the wintertime EA coastal trough, but in terms of increasing the temperature and thickness of the troposphere above. The strongest signal of predictability came from the northwestern Atlantic; it corresponds to the northern part of the tripole SST anomaly associated with the negative North Atlantic Oscillation (NAO) phase, i.e., a positive SLP anomaly in the Icelandic low area. Such configuration of SLP anomalies precedes winters with a positive AO polarity (Kryjov, 2015), i.e., a tendency toward the positive northern EAT anomaly.

Time series of observed and predicted anomalies of the EAT PC1 in respect to the preceding 25 year training periods are shown in Figure 3.3.4. The TCC between the series is 0.44, MSSS is 0.19. The predicted series reflect the general features of the observed series. However, it does not reproduce observed extremes. It is an inherent shortcoming of regressions (Wilks, 1995).

Projection of the DJF EAT predicted PC1 onto the loading pattern of EOF1 yields the forecast fields of EAT anomalies. Although these fields are composed with the only EOF1, we verify them against the original fields of the anomalies. The maps of TCC and MSSS are shown in Figure 3.3.5. The most skillful predictions are over eastern Mongolia and western Manchuria. For most of Korean Peninsula TCC is within 0.3-0.5 and MSSS is above zero, which indicates that for Korea the developed prediction method outperforms climatological forecast.

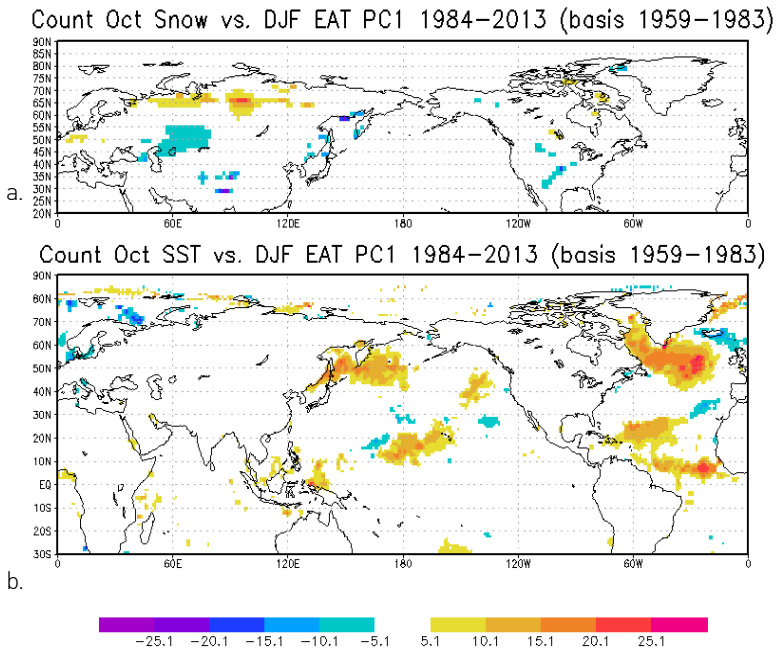

Figure 3.3.3 The number of forecasts (out of 30) with absolute values of the correlation coefficient between the DJF EAT PC1 and October snow cover (a) and SST (b) exceeding 0.4; positive (negative) values correspond to positive (negative) correlation coefficients. The numbers with absolute values exceeding five are significant at the 99% confidence level based on tests with the binomial probability distribution.

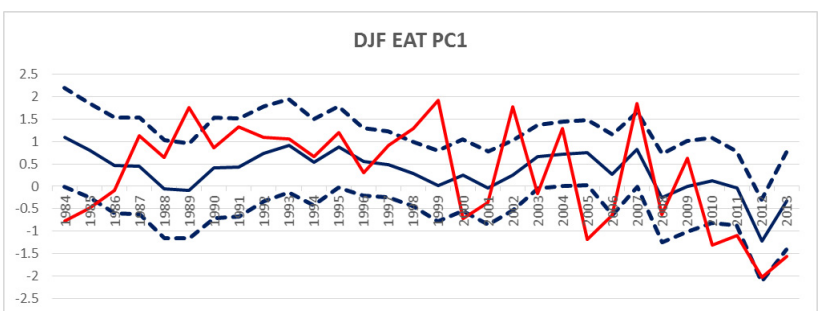

Figure 3.3.4 Time series (solid lines) of observed (red) and predicted (blue) anomalies of EAT PC1 in respect to the preceding 25-year training periods. Dashed lines depict the 95% confidence intervals of the predicted series.

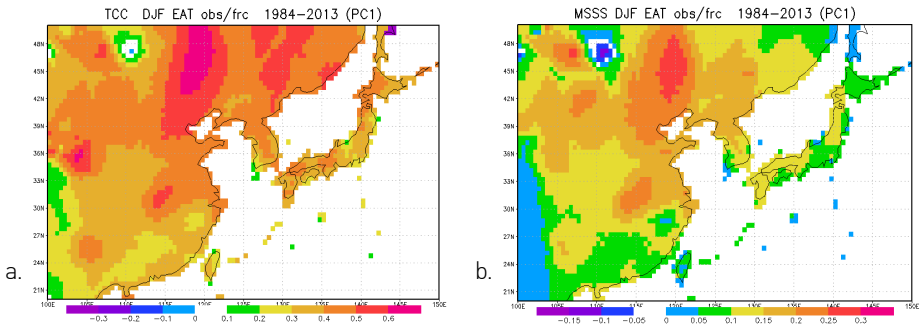

Figure 3.3.5 The TCC (a) and MSSS (b) of the predictions of DJF EAT based on forecasts of the DJF EAT PC1.

3.3.1.2 Prediction of East Asia temperature EOF2

The second EOF (Figure 3.3.6) explains 21% of the total variance of DJF EAT. It is a dipole South – North (we selected the positive polarity which provides positive loadings over Korea). EOF2 loadings in terms of correlations between the PC2 (Figure 3.3.7) and gridpoint temperature series are within 0.2 – 0.4 over Korea. It indicates that contribution of EOF2 to Korea temperature is rather small, much less than that of EOF1. Anyway, skillful prediction of EOF2 may contribute to the skill of the forecasts.

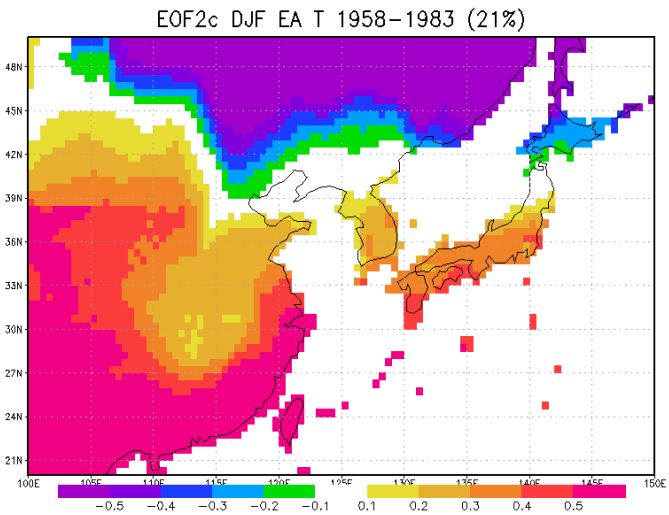

Figure 3.3.6 The DJF EAT EOF2 shown as a correlation map between temperature fields and PC2.

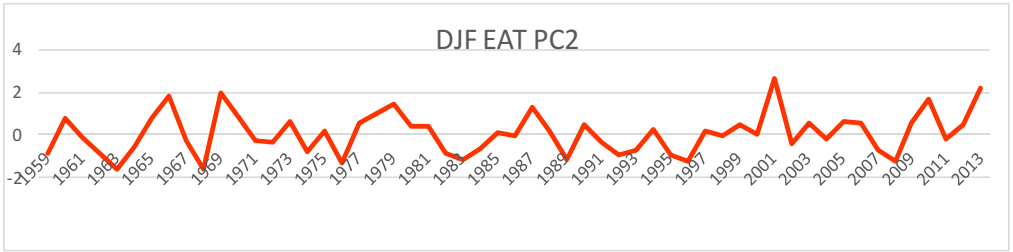

Figure 3.3.7 Time series of the PC1 for the DJF EAT.

The Z500 fields based predictors have been selected (Fig. 3.3.8) out of six potential ones listed above. The positive phase of the DJF EAT PC2 tends to be preceded by the positive Z500 anomaly over the Kara Sea – Taymyr Peninsula and negative Z500 anomalies over the Okhotsk Sea and north-eastern North America. It resembles the inverted predictors of the DJF AO. Indeed, correlation between the DJF AO and PC2 is 0.53.

Time series of observed and predicted anomalies of EAT PC2 are shown in Figure 3.3.9. TCC between the series is 0.50, MSSS is 0.25.

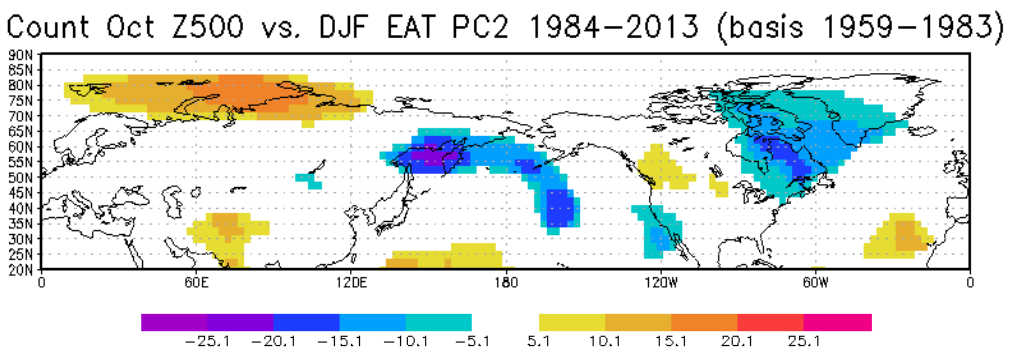

Figure 3.3.8 The number of forecasts (out of 30) with absolute values of the correlation coefficient between the DJF EAT PC2 and October Z500 exceeding 0.4; positive (negative) values correspond to positive (negative) correlation coefficients. The numbers with absolute values exceeding 5 are significant at the 99% confidence level based on tests with the binomial probability distribution.

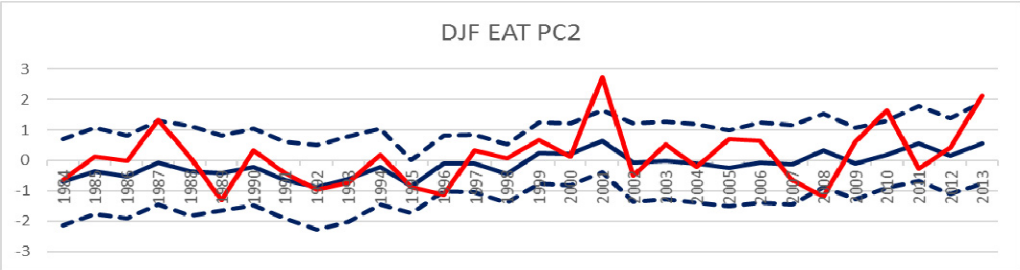

Figure 3.3.9 Time series (solid lines) of observed (red) and predicted (blue) anomalies of EAT PC2 in respect to the preceding 25-year training periods. Dashed lines depict the 95% confidence intervals of the predicted series.

Projection of the DJF EAT predicted PC2 onto the loading pattern of EOF2 yields the forecast fields of EAT anomalies associated with EOF2. A predicted EAT field is a summation of the EOF1 and EOF2 associated fields. Verification of the obtained fields against the original fields of the anomalies yields results shown in Figure 3.3.10. It is noticeable general slight improvement over China as compared with EOF1 alone. For most of Korean Peninsula TCC is within 0.3-0.5 and MSSS is above zero. This indicates that, on the one hand, for Korea the developed prediction method outperforms climatological forecast, on the other hand, however, as compared with EOF1 only, for Korea it is noticeable slight (within confidence intervals) deterioration.

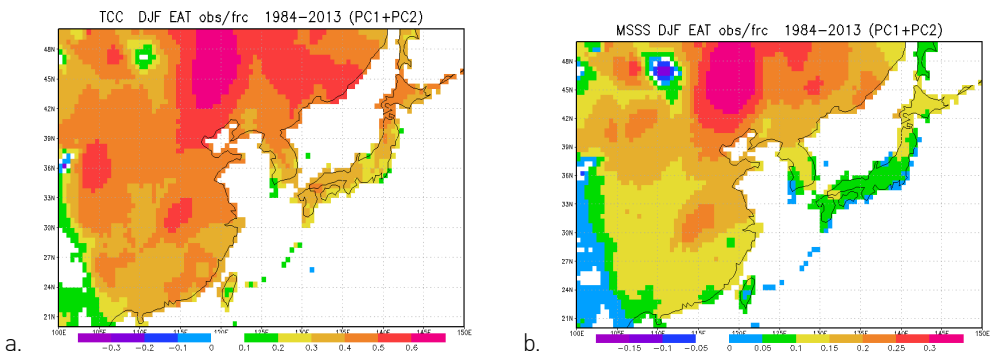

Figure 3.3.10 The TCC (a) and MSSS (b) of the predictions of DJF EAT based on forecasts of the DJF EAT PC1 and PC2.

3.3.1.3 Prediction of East Asia temperature EOF3

The EOF3 of East Asia DJF temperature (10% of variance explained) is shown in Fig. 3.3.11 as a correlation map between temperature fields and PC3. It is (roughly) a WEST – EAST dipole pattern. Correlations between the PC3 and Korea gridpoint temperature series are presumably within 0.5 – 0.6.

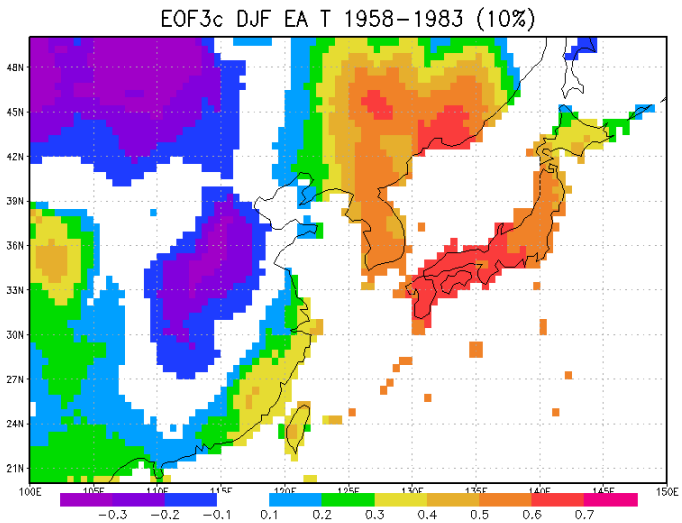

Figure 3.3.11 The DJF EAT EOF3 shown as a correlation map between temperature fields and PC3.

The PC3 time series is shown in Fig. 3.3.12. It is just the component of the DJF EAT series which contributes the shift to warm winters between 1986 and 1987. However, an epoch of warm winters ended or, at least, was interrupted in 2011.

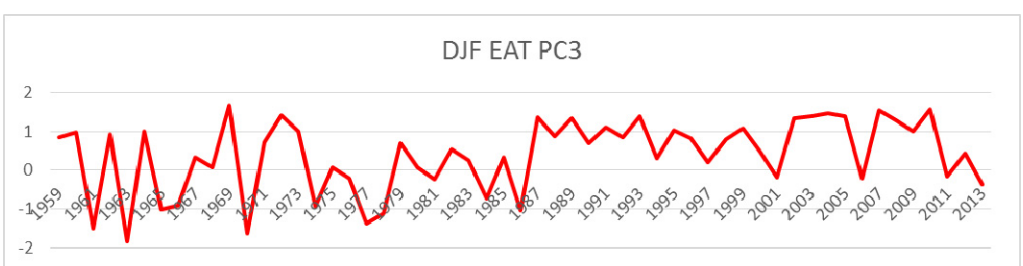

Figure 3.3.12 Time series of the PC3 for the DJF EAT.

Selection of the predictors to the PC3 yields the SST field (Fig. 3.3.13) with TCC and MSSS between the observed and predicted PC3 series being 0.40 and 0.10, correspondingly. The method of construction of predictor developed in this study has appeared flexible enough for prediction of the PC3 increase in the late 1980s and PC3 decrease in the early 2010s in real-time mode predictions (Fig.3.3.14).

Verification assessments of the DJF EAT represented by summation of forecasts of three leading EOFs is shown in Figure 3.3.15. In spite of quite low contribution of the EOF3 to total EAT variance, its improvement is well noticeable throughout almost the whole region of East Asia. Particularly, TCC and MSSS of the forecasts of wintertime temperature are for Korean Peninsula 0.40 – 0.60 and 0.20 – 30, correspondingly. For East Asia in the large regions TCC exceeds 0.60 and MSSS exceeds 0.3.

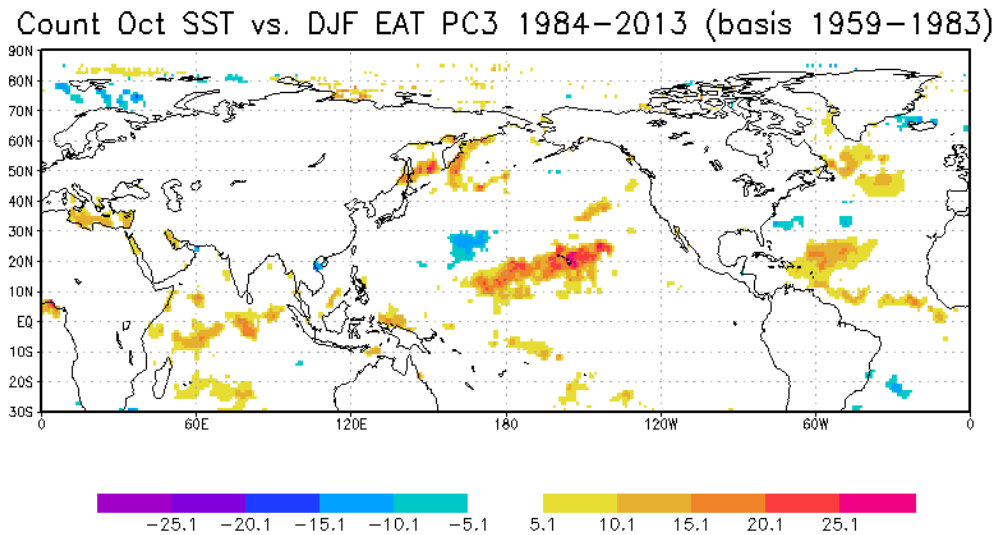

Figure 3.3.13 The number of forecasts (out of 30) with absolute values of the correlation coefficient between the DJF EAT PC3 and October SST exceeding 0.4; positive (negative) values correspond to positive (negative) correlation coefficients. The numbers with absolute value exceeding 5 are significant at the 99% confidence level in the test based on Binomial probability distribution.

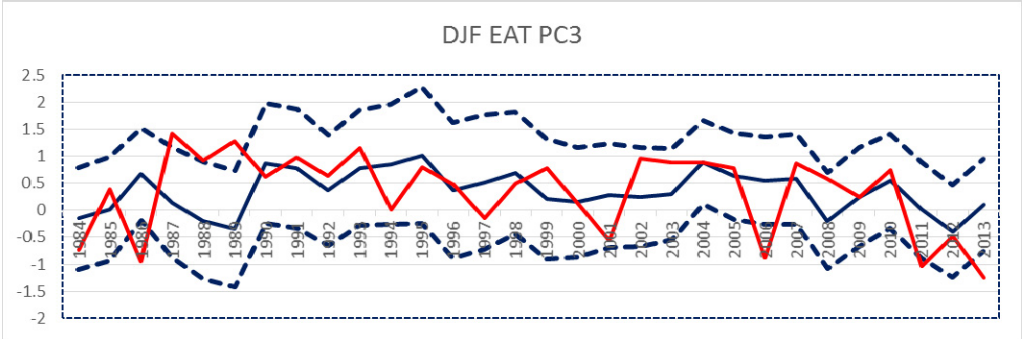

Figure 3.3.14 Time series (solid lines) of observed (red) and predicted (blue) anomalies of EAT PC3 in respect to the preceding 25-year training periods. Dashed lines depict the 95% confidence intervals of the predicted series.

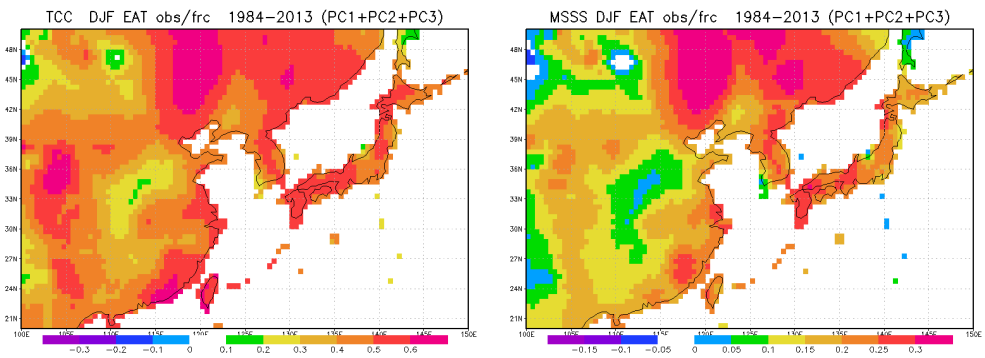

Figure 3.3.15 The TCC (a) and MSSS (b) of the predictions of DJF EAT based on forecasts of the DJF EAT PC1, PC2, and PC3.

3.3.1.4 Concluding remarks

The carried out study has shown the success of the developed statistical tool, the statistical “engine” of the physical-empirical model, in both a single predictor option as in prediction of the DJF AOI described in Section 3.2 and a multi-predictor option applied for prediction of EAT PC1.

It is worth noting, that both abrupt increase of EAT between 1986 and 1987 and decrease in the 2010s are reflected in the DJF EAT PC3. Both appear well predictable (at least as tendencies) in the real-time mode, i.e., with regression equation being derived on 25-year series preceding the forecast years, with the “shift” years

being among them. It suggests that the mentioned abrupt changes are rather statistical phenomena than real climatological shifts.

3.3.2 Prediction of South Korea Temperature Fields

The first EOF of South Korea wintertime temperature is shown in Fig. 3.3.16 as correlations between the corresponding series of PC1 (Fig. 3.3.17) and the gridpoint temperature series. It is almost homogeneous. The correlation coefficients are above 0.95 for all the points with just few exceptions. The first EOF mode accounts for 95% of total variance. The PC1 is closely related to South Korea average temperature, with correlation between them being 0.99. By means of stepwise multiple regression (please see Appendix 1 for explanation of the prediction technique) we have selected two predictors of South Korea temperature PC1, those based on SIC and SST.

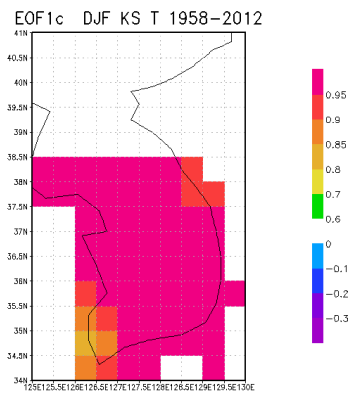

Figure 3.3.16 The EOF1 of South Korea wintertime temperature.

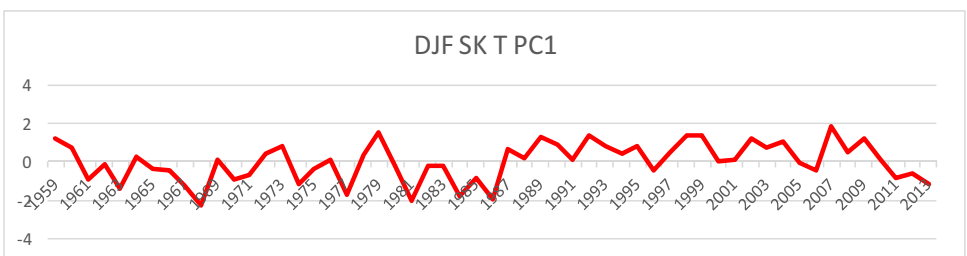

Figure 3.3.17 The PC1 of South Korea wintertime temperature.

We performed 30 predictions, the number of forecasts (out of 30) with an absolute value of the correlation coefficient between DJF KST PC1 and October SIC (a) and SST (b) exceeding 0.40 is shown in Fig. 3.3.18. For positive DJF temperature PC1 positive anomaly favorable is enhanced SIC in the Northern Barents and Kara seas (Fig. 4.18a) with corresponding negative anomalies of SST in the same region (Fig. 3.3.18b). These correlations are consistent with results from previous studies (e.g., Chen et al., 2014) showing that for positive (negative) anomaly of East Asia wintertime temperature favorable is positive (negative) anomaly of SIC in preceding autumn. Possible mechanism could reside in the positive feedback between the negative (positive) anomalies of surface temperature (positive SIC and negative SST (negative SIC and positive SST)) in the northern Barents and Kara seas and negative (positive) anomaly of geopotential and SLP downstream, over the Taymyr peninsula, which, in turn, drives advection of warm (cold) air to East Asia weakening (enhancing) East Asia Trough. Strong correlations with surface properties and insignificant correlations with circulation characteristics could be explained by a stronger noise in the series of circulation characteristics as compared to series of surface properties.

a.

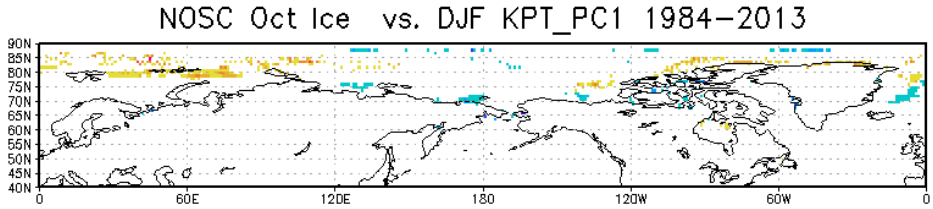

b.

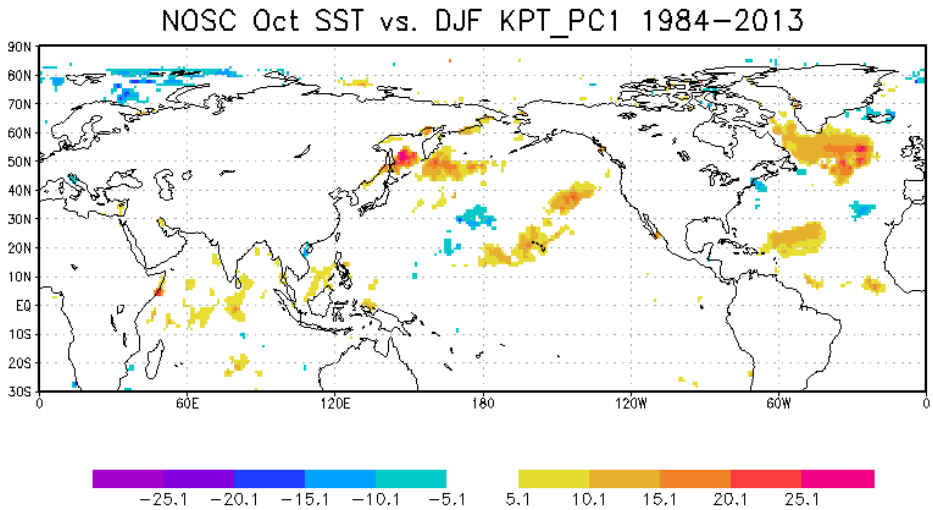

Figure 3.3.18 The number of forecasts (out of 30) with absolute values of the correlation coefficient between the DJF KST PC1 and October SIC (a) and SST (b) exceeding 0.4; positive (negative) values correspond to positive (negative) correlation coefficients. The numbers with absolute values exceeding five are significant at the 99% confidence level based on tests with the binomial probability distribution.

It should be noted that areas of strong KST-SST relationships are not restricted to only the northern Barents and Kara seas. Particularly, high frequency of the predictors occurs in the Okhotsk Sea and eastward from it, i.e., the area below the East Asia trough, and western North Atlantic where the pattern resembles the negative NAO associated SST tripole preceding the positive wintertime KST anomaly as well as the positive DJF AO polarity.

The skill of the forecasts of DJF KST PC1 is characterized by TCC = 0.41 and MSSS = 0.12 (Fig. 3.3.19), with the multiple correlation coefficient averaged over those obtained on 30 training periods being 0.84. Since PC1 explains the temperature variations of the same phase throughout almost whole South Korea, the spatial (pattern) correlation coefficient reflects whether the sign of the anomalies prevailing throughout the whole South Korea is predicted correctly or not.

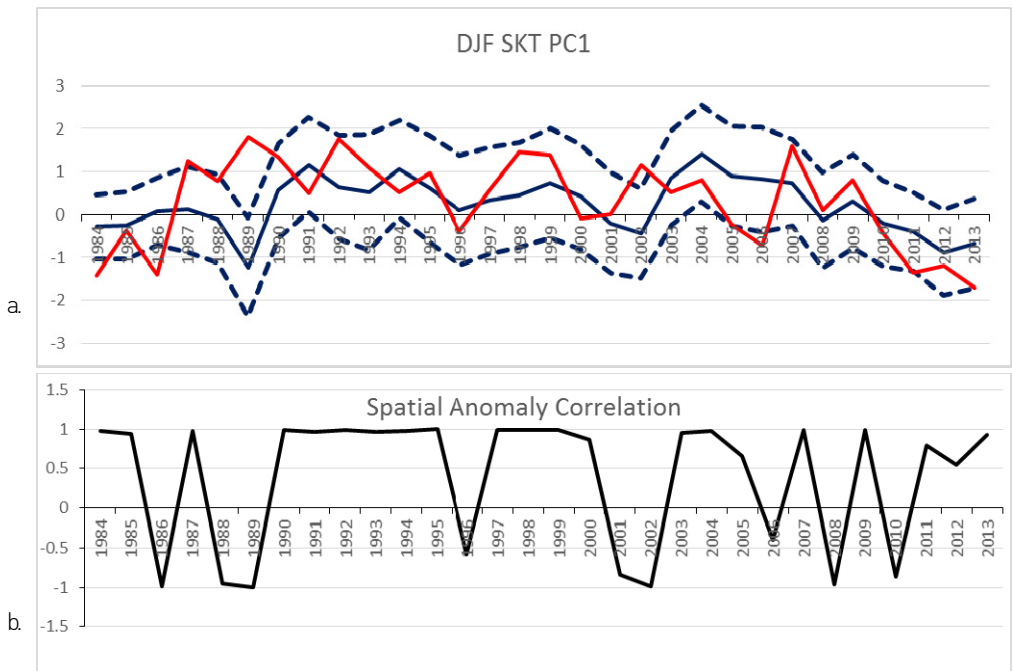

Figure 3.3.19 (a) Time series of observed (red) and predicted (blue) DJF KST PC1 values. Years as of January. Dashed lines – 95% confidence intervals of predicted values. (b) Time series of spatial anomaly correlations between observed and predicted fields of KST.

The skill of DJF temperature over South Korea (Figure 3.3.20) predicted as a forecast of PC1 is characterized by TCC above 0.40-0.50 above the whole South Korea with an exception of the very south-western region of the peninsula where TCC is between 0.3 and 0.4. It means that the newly developed method outperforms prediction by downscaling from the multi-model forecasts (Min et al., 2011) shown in Fig. 3.3.20c.

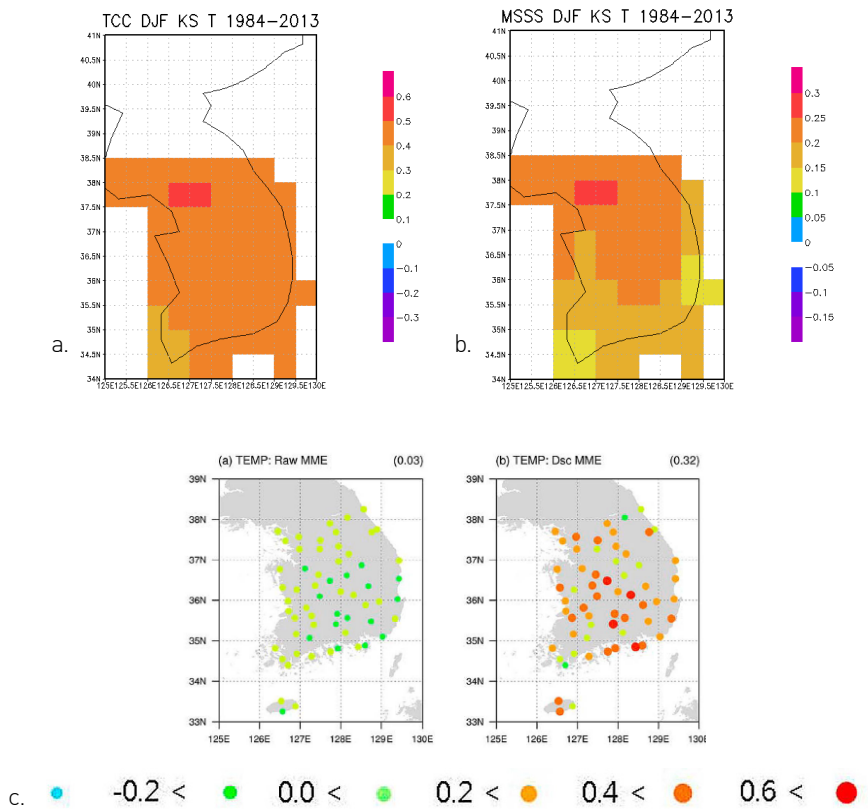

Figure 3.3.20 The TCC (a) and MSSS (b) of the forecasts of wintertime temperature based on the forecasts of PC1. (c) The TCC of raw and downscaled APCC MME forecasts of wintertime temperature (Min et al., 2011, Figure 4).

3.3.3 Prediction of Korean Peninsula Temperature Fields

For the Korean Peninsula as a whole, results are similar to those obtained for South Korea. The best skill is provided by multiple regression based combination of SIC and SST predictors. For most of the peninsula TCC is within the range 0.4 – 0.5 and MSSS is within 0.15 – 0.30 (Fig. 3.3.21).

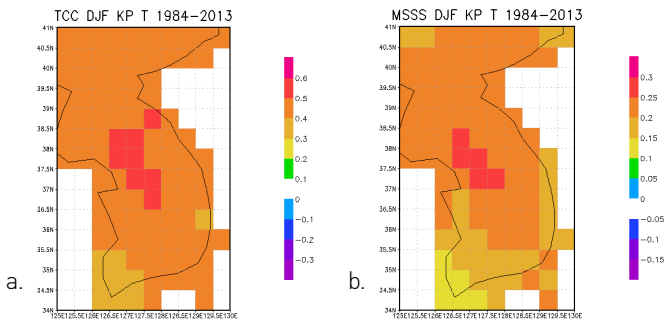

Figure 3.3.21 The TCC (a) and MSSS (b) of the forecasts of wintertime temperature based on the forecasts of PC1.

3.3.4 Prediction of South Korea Temperature Fields in Cross-Validation Mode: Examples

We perform 25 cross-validated predictions (3 years withheld) of EAT, KST, and KPT. The obtained skill scores are, in general, slightly higher than those for real-time forecasts which supports the results obtained on the real-time forecasts. However, the performed analysis revealed shortcoming of the use of cross-validation for verification assessments of the statistical forecasts. We analyze this shortcoming taking prediction of the KST field as an example.

Prediction procedure is similar to that of the real-time forecast. We select the best predictors with the use of various variables in both single and multiple regression. The best results were obtained with the use of SIC fields as a basis for construction of predictors. The map of the numbers of forecasts (out of 25) with an absolute value of the correlation coefficient between the DJF KST PC1 and October SIC exceeding 0.4 is shown in Figure 3.3.22. Positive (negative) values correspond to positive (negative) correlation coefficients. The shown map is consistent with the

results of Chen et al. (2014) and it closely qualitatively resembles the map obtained in the real-time mode shown in Fig. 3.3.18a. What differs it from the latter is a clearly manifested high stability of the strongest predictor-contributing points throughout all the 25 forecasts. It looks unrealistically for real-time forecasts (please compare with Fig. 3.3.18a).

Time series of observed and predicted anomalies of KST PC1 are shown in Figure 3.3.23. TCC between the series is 0.57 (0.41 for real-time forecasts), MSSS is 0.32 (0.12 for real-time forecast). This "improvement" is mainly due to change in the forecasting/verification procedure.

Projection of the predicted DJF KST PC1 onto the loading pattern of EOF1 yields the forecast fields of KST anomalies associated with EOF1. Quite expectedly, verification of the obtained fields against the original fields of the anomalies yields high results shown in Figure 3.3.24. For most of South Korea TCC is within 0.5-0.6 and MSSS is above 0.3. This TCC score essentially outperforms all other TCCs obtained in the verification procedures based on the real-time forecasting scheme. However, we cannot consider it realistic and appropriate for our study.

We have also tested prediction skill on the series stratified according the October-February mean index of the PDO referring to Wang et al. (2008) who showed modulation of the ENSO impact on EAWM by the PDO. Qualitatively, predictions during the negative PDO phase are more skillful than during the positive PDO phase (TCC = 0.61 and 0.52, correspondingly) which corresponds to Wang et al. (2008) results. However, this difference is statistically insignificant at the 5% level. Further investigations on the longer series should be performed.

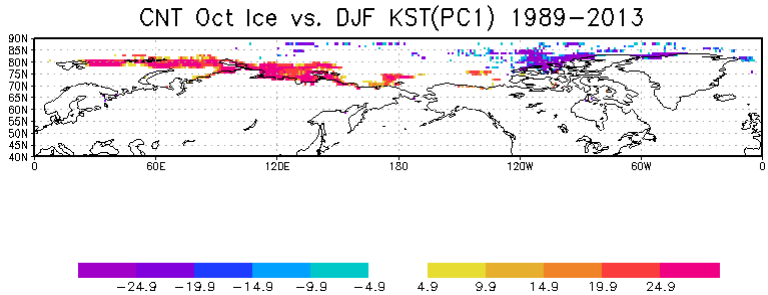

Figure 3.3.22 The number of forecasts (out of 25) with absolute values of the correlation coefficient between the DJF KST PC1 and October sea ice concentration exceeding 0.4; positive (negative) values correspond to positive (negative) correlation coefficients. The numbers with absolute values exceeding 5 are significant at the 99% confidence level based on tests with the binomial probability distribution.

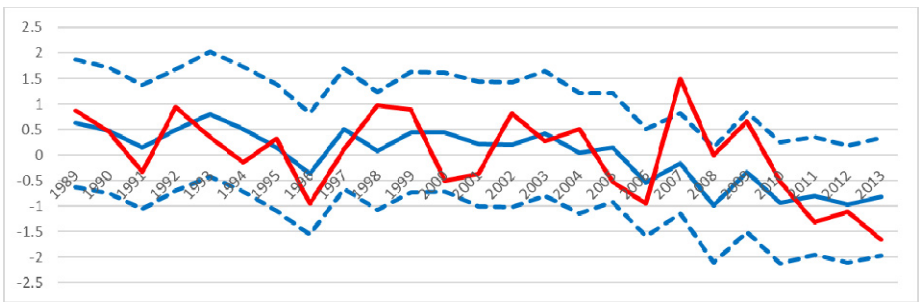

Figure 3.3.23 Time series (solid lines) of observed (red) and predicted (blue) anomalies of EAT PC2 in respect to the preceding 25-year training periods. Dashed lines depict the 95% confidence intervals of the predicted series.

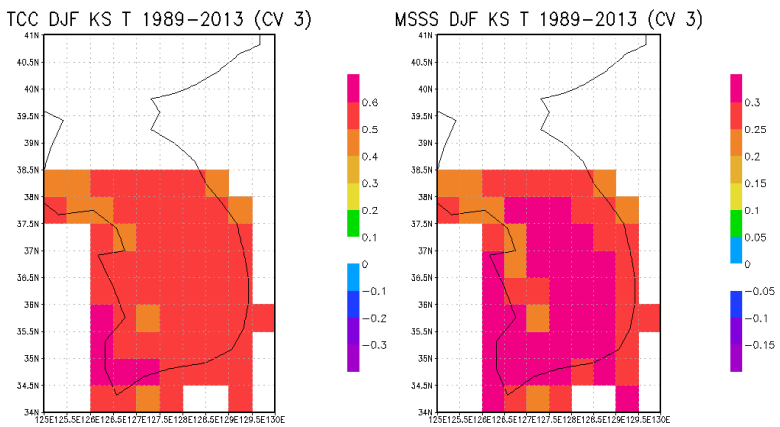

Figure 3.3.24 The TCC (a) and MSSS (b) of the forecasts of DJF KST derived as predictions of the PC1 of the DJF KST fields.

3.4 Prediction of the East Asia Winter Monsoon Indices

More than ten East Asia Winter Monsoon indices (EAWMI) have been suggested so far. They characterize wintertime monsoon (circulation and response of various variables) from various points of view and are based on various circulation characteristics. Particularly, EAWMIs of Juhn and Lee (2004) and Li and Yang (2010) are based on the meridional gradients of the zonal wind in the upper troposphere – lower stratosphere. A number of indices are based on the mid-troposphere circulation anomalies (e.g., Sun and Lee (1997), Cui and Sun (1999), Wang et al. (2009); and on the SLP anomalies (Wang and Chen, 2014).

Predictability of most of these indices by the APCC models has been assessed by Shin (APCC Report, 2014). The highest prediction skill (TCC=0.59) has been performed by the POAMA model in prediction of the wintertime EAWMI suggested by Wang and Chen (2014). It is worth reminding that it is a combination of normalized SLP series representing gradients Siberian high – western North Pacific and Siberian high – Maritime continent. Normalization of SLP series with a corresponding implicit increase of the Maritime continent SLP variability up to that of the extratropical areas make it the most predictable by the seasonal dynamic models skillfull in the tropics and less skillful in the extratropics.

We have analyzed statistical predictability and stability of the relationships of DJF KST with all the EAWMIs considered by Shin (2014) with addition of two more indices, a EAWMI suggested by Jhun and Lee (2004) and a EAWMI estimated as an SLP gradient between the western North Pacific and northern Siberian high (SLP[25-35N, 140-170E] – SLP[50-65N, 60-110E]) which is not described in the papers but could be suggested based on Fig. 3.1.7d. Results are quite similar. Correlations in the 25-year sliding windows vary within 0.6 – 0.9. These deviations do not exceed the 95% confidence intervals and may be considered as occasional. As example, we show here results from analysis for three indices (Fig. 3.3.25).

Predictability of the indices is similar to or slightly lower than that of DJF KST in real-time forecasts (TCC = 0.3 – 0.5). It means that it is not reasonable to predict DJF KST using the DJF EAWMIs as intermediate predictors. Nonetheless, what makes sense in operational forecasting is prediction of the EAWMIs as an indirect support

for the predicted DJF KST anomalies.

Also, the analysis provides additional support of the conclusions from Section 3.3.4 that verification assessments performed by cross-validation scheme tend to overestimate the skill of tested statistical models. Both TCCs and MSSSs obtained on cross-validated forecasts of the EAWMIs are essentially higher than those from real-time-simulated forecasts.

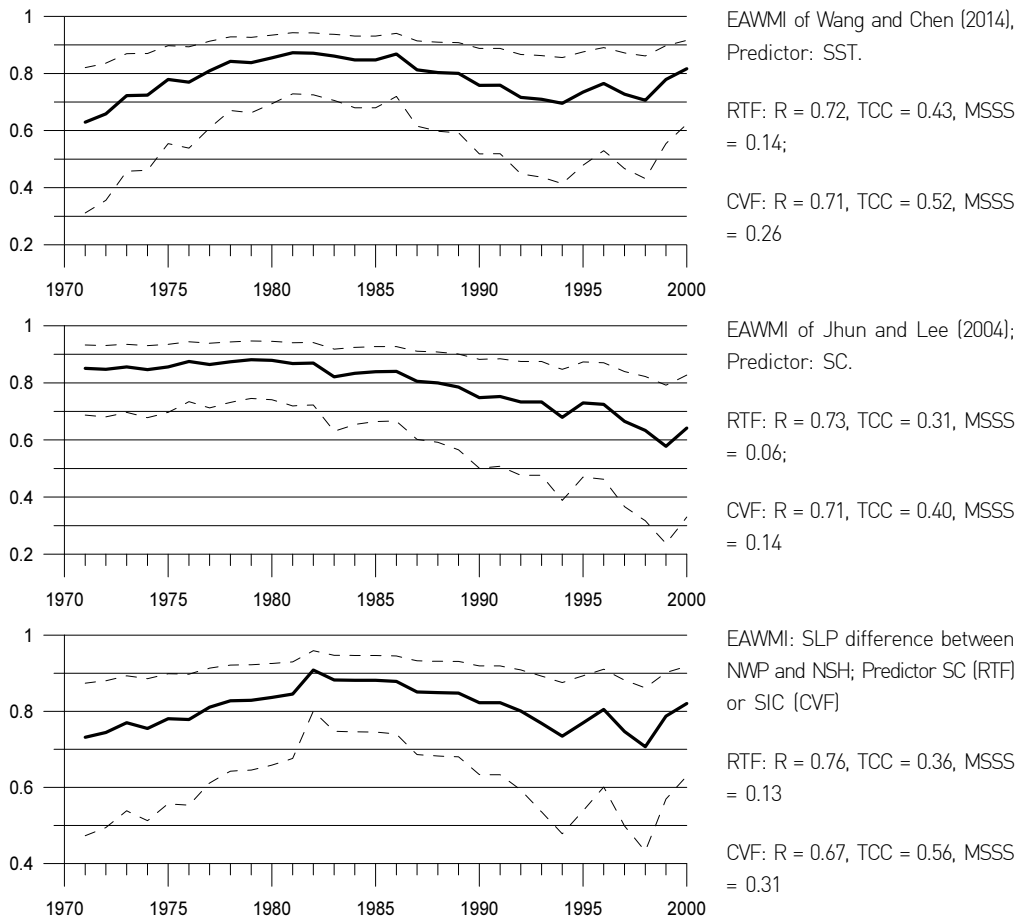

Figure 3.3.25 Correlation coefficients for the sliding 25-year windows between DJF KST and the DJF EAWM indices: (a) Wang and Chen (2014); (b) Jhun and Lee (2004); (c) SLP difference between NW Pacific and SH. In the right panel shown are predictability characteristics for real-time (RTF) and 3-year-out cross-validated (CVF) forecasts. R is mean correlation coefficient averaged over 30 for RTF (25 for CVF) correlation coefficients underlying regression equations.

3.5 Preliminary Tests: Wintertime Monthly Temperature and Seasonal Total Precipitation

A test of prediction of wintertime monthly temperature have been conducted. For each month the leading predictors were selected independently upon other months because of intraseasonal variations of the teleconnections (Kim et al., 2015). The skill of the forecasts is rather low which is usual for monthly forecasts, both statistical and numerical. In our particular case, prediction of monthly temperature with not less than one month lead has yielded no significant result. In cross-validation mode, there are numerically valid results (Table 3.5.1) but there is a high probability of overestimation (please see sections 3.3.4 and 3.3.5).

Table 3.5.1 Verification assessments of forecasts (1989–2013) for wintertime monthly KST performed in cross-validation mode with three years withheld.

Predictand	Predictor	R training periods	TCC	MSSS
December KST	October SIC	0.71	0.46	0.14
	October SST	0.73	0.37	0.09
January KST	October SIC	0.59	0.46	0.20
	October Z500	0.58	0.42	0.15
February KST	October Z300	0.60	0.29	0.03
	December SST	0.80	0.36	0.08

We have performed the tests of prediction of wintertime precipitation anomalies. However, the skill is modest (Table 3.5.2).

Table 3.5.2 Verification assessments of forecasts (1989-2013) of wintertime total seasonal precipitation averaged over South Korea (KSP) and the Korean Peninsula (KPP) performed in real-time mode (RTF) and cross-validation mode (CVF) with three years withheld.

Predictand	Predictor/mode	R training periods	TCC	MSSS
KSP	Z300/RTF	0.62	0.17	-0.09
	Z300/CVF	0.67	0.26	-0.01
KPP	Z300/RTF	0.61	0.19	-0.07
	Z300/CVF	0.60	0.32	0.05

4. CONCLUDING REMARKS

This study has been aimed on development of self-tuning physical-empirical (statistical) models for seasonal prediction of wintertime temperature over East Asia, particularly South Korea, appropriate for using at APCC operational practice as a support and complement to APCC MME forecasts.

A statistical tool underlying the self-tuning physical-empirical models has been developed. It is based on multiple regression scheme with flexible construction of the predictors. Tests performed on prediction of the wintertime AO index in real-time forecasting mode on independent data have demonstrated its efficiency. The independently constructed predictors affect the wintertime AO through clear physically plausible mechanisms described in relevant papers. The based on the same statistical tool physical-empirical models for prediction of East Asia wintertime temperature confirm efficiency of the developed tool providing construction of physically plausible predictors, revealed in the pre-prediction study and described in literature, and skillful forecast.

The results from experiments with forecasting in real-time mode for 30 winters (1983/84-2012/13):

- DJF AOI: TCC exceeds 0.60 and MSSS exceeds 0.35 which is the skill level of two world best AOI forecasting dynamic models;
- DJF EAT: three leading PCs (>80%) are predicted with TCC = 0.40 - 0.50, MSSS = 0.10 – 0.25 which provides the prevailing level of South Korea gridpoint skill of TCC = 0.40 - 0.60 and MSSS = 0.20 – 0.30;
- Korean Peninsula and South Korea wintertime KPT and KST: PC1s (93% & 95%) are predicted with MSSS>0.10, TCC=0.40-0.45 which provides the prevailing gridpoint skill of TCC = 0.40 – 0.50 MSSS > 0.10, which outperforms existing MMEs (TCC = 0.10 – 0.30).

This obtained skill for South Korea wintertime temperature is provided mainly by the extratropical predictors originated from the extratropical processes . Another impact comes from the tropics. It is (at least directly) weakly accounted for in the developed method. Therefore, it is reasonable to combine forecasts from the developed physical-empirical models with seasonal forecasts from the dynamic models which are mainly governed by the tropical SST anomalies.

REFERENCES

Ahn, J.B., and H.J. Kim, 2013: Improvement of 1-month lead predictability of the wintertime AO using a realistically varying solar constant for a CGCM. Meteorological Applications **21**: 415–418, doi: 10.1002/met.1372.

Camp, C.D., and K.K. Tung, 2007: Stratospheric polar warming by ENSO in winter: A statistical study. Geophysical Research Letters **34:** L04809, doi: 10.1029/2006GL028521.

Chang, C.P., and M.M. Lu, 2012: Intraseasonal predictability of Siberian High and East Asian winter monsoon and its inter-decadal variability. Journal of Climate **25**: 1773–1778.

Cheung, H.N., W. Zhou, H.Y. Mok, M.C. Wu, 2012: Relationship between Ural–Siberian Blocking and the East Asian Winter Monsoon in Relation to the Arctic Oscillation and the El Nin˜ o–Southern Oscillation. Journal of Climate **25**: 4242–4257.

Chen, Z., R. Wu, W. Chen, 2014: Impacts of Autumn Arctic Sea Ice Concentration Changes on the East Asian Winter Monsoon Variability. Journal of Climate **27**: 5433-5450

Clark, M.P., and M.P. Serreze, 2000: Effects of variations in East Asian snow cover on modulating atmospheric circulation over the North Pacific Ocean. Journal of Climate **13**: 3700–3710

Cohen, J., M. Barlow, P. Kushner, and K. Saito, 2007: Stratosphere–troposphere coupling and links with Eurasian land surface variability. Journal of Climate **20**: 5335–5343, doi: 10.1175/2007JCLI1725.1.

Cohen, J., and C. Fletcher, 2007: Improved skill of Northern Hemisphere winter surface temperature prediction based on land–atmosphere fall anomalies. Journal of Climate **20**: 4118–4132.

Cohen, J., and J. Jones, 2011: A new index for more accurate winter predictions. Geophysical Research Letters **38**: L21701, doi: 10.1029/2011GL049626.

Compo, G.P., J.S. Whitaker, and P.D. Sardeshmukh, 2006: Feasibility of a 100 year reanalysis using only surface pressure data. Bulletin of the American Meteorological Society **87**: 175–190.

Compo, G.P., J.S. Whitaker, P.D. Sardeshmukh, and coauthors, 2011: The Twentieth Century Reanalysis Project. Quarterly Journal of the Royal Meteorological Society **137:** 1–28, doi: 10.1002/qj.776.

Cui, X., and Z. Sun, 1999: East Asian winter monsoon index and its variation analysis. Journal of Nanjing Institute of Meteorology **22**, 321–325.

Folland, C.K., A.A. Scaife, J. Lindesay, and D.B. Stephenson, 2012: How potentially predictable is northern European winter climate a season ahead? International Journal of Climatology **32**: 801–818, doi: 10.1002/joc.2314.

Garfinkel, C.I., D.L. Hartmann, and F. Sassi, 2010: Tropospheric precursors of anomalous Northern Hemisphere stratospheric polar vortices. Journal of Climate **23:** 3282–3299.

Gong, D.Y., S.W. Wang, J.H. Zhu, 2001: East Asian winter monsoon and Arctic Oscillation. Geophysical Research Letters **28**, 2073-2076.

Harris, I., P.D. Jones, T.J. Osborn, and D.H. Lister, 2014: Updated high-resolution grids of monthly climatic observations – the CRU TS3.10 Dataset. International Journal of Climatology **34**: 623–642, doi: 10.1002/joc.3711.

Holton, J.R., 2004: An introduction to Dynamic Meteorology. Fourth edition. Elsevier Academic Press: San Diego, CA.

Jeong, J.H., and C.H. Ho, 2005: Changes in occurrence of cold surges over east Asia in association with Arctic Oscillation. Geophysical Research Letters **32,** L14704, doi:10.1029/2005GL023024

Jhun, J.G., and E.J. Lee, 2004: A new East Asian winter monsoon index and associated characteristics of the winter monsoon. Journal of Climate **17**: 711–726.

Kalnay, E., and coauthors, 1996: The NCEP/NCAR 40-year reanalysis project. Bulletin of the American Meteorological Society **77:** 437–471.

Kang, D., M.I. Lee, J. Im, D. Kim, H.M. Kim, H.S. Kang, S.D. Schubert, A. Arribas, and C. MacLachlan, 2014: Prediction of the Arctic Oscillation in boreal winter by dynamical seasonal forecasting systems. Geophysical Research Letters **41**: 3577–3585, doi: 10.1002/2014GL060011.

Kim, G., J.B. Ahn, V.N. Kryjov, S.J. Sohn, W.T. Yun, R. Graham, R.K. Kolli, A. Kumar, and J.P. Ceron, 2015a: Global and regional skill of the seasonal predictions by WMO Lead Centre for Long-Range Forecast Multi-Model Ensemble. International Journal of Climatology, doi: 10.1002/joc.4449.

Kim, S., H.S. Kim, S.K. Min, H.Y. Son, D.J. Won, H.S. Jung, and J.S. Kug, 2015b: APJAS, Intra-winter atmospheric circulation changes over East Asia and North Pacific associated with ENSO in a seasonal prediction model. Asia-Pacific Journal of Atmospheric Sciences **51**: 49–60, doi: 10.1007/s13143-014-0059-9.

Kryjov, V.N., 2015: October circulation precursors of the wintertime Arctic Oscillation. International Journal of Climatology **35**: 161–171, doi: 10.1002/joc.3968.

Kryjov, V.N., Y.M. Min, 2016: Predictability of the Wintertime Arctic Oscillation Based on Autumn Circulation. International Journal of Climatology, Wiley online library, doi: 10.1002/joc.4616.

Kryjov, V.N., and C.K. Park, 2007: Solar modulation of the El-Niño/Southern Oscillation impact on the Northern Hemisphere annular mode. Geophysical Research Letters **34**: L10701, doi: 10.1029/2006GL028015.

Kryzhov, V.N., 2012: Downscaling of the global seasonal forecasts of Hydrometcenter of Russia for North Eurasia. Russian Meteorology and Hydrology, **37**: 291-297

Kug, J.S., J.Y. Lee, and I.S. Kang, 2008: Systematic error correction of dynamical seasonal prediction of sea surface temperature using a stepwise pattern projection method. Monthly Weather Review **136**: 3501–3512, doi: 10.1175/2008MWR2272.1.

Lee, J.Y., S.S. Lee, B. Wang, K.J. Ha, and J.G. Jhun, 2013a: Seasonal prediction and predictability of the Asian winter temperature variability. Climate Dynamics **41**: 573–587, doi: 10.1007/s00382-012-1588-5.

Lee, S.S., S.H. Kim, J.G. Jhun, K.J. Ha, and Y.W. Seo, 2013b: Robust warming over East Asia during the boreal winter monsoon and its possible causes. Environmental Research Letters **8**: 034001.Li, Y., and S. Yang, 2010: A dynamical index for the East Asian winter monsoon. Journal of Climate **23**: 4255–4262.

Liu, J., Z. Zhang, R.M. Horton, C. Wang, X. Ren, 2007: Variability of North Pacific Sea Ice and East Asia–North Pacific Winter Climate. Journal of Climate **20**: 1991–2001.

MacLachlan, C., A. Arribas, K.A. Peterson, and coauthors, 2014: Global Seasonal forecast system version 5 (GloSea5): a high-resolution seasonal forecast system. Quarterly Journal of the Royal Meteorological Society 141: 1072–1084, doi: 10.1002/qj.2396.

Min, Y.-M., V.N. Kryjov, and J.-H. Oh, 2011: Probabilistic interpretation of regression-based downscaled seasonal ensemble predictions with the estimation of uncertainty. Journal of Geophysical Research **116**: D08101, doi: 10.1029/2010JD015284.

Min, Y.-M., V.N. Kryjov, and S.M. Oh, 2014: Assessment of APCC multi-model ensemble prediction in seasonal climate forecasting: Retrospective (1983–2003) and real-time forecasts (2008–2013). Journal of Geophysical Research-Atmospheres **119**(21): 12,132–12,150, doi: 10.1002/2014JD022230.

Murphy, A.H., 1988: Skill scores based on the mean squared error and their relationships to the correlation coefficient. Monthly Weather Review **116**: 2417–2424.

Park, H.J., and J.B. Ahn, 2015: Combined effect of the Arctic Oscillation and the Western

Pacific pattern on East Asia winter temperature. Climate Dynamics, doi: 10.1007/s00382-015-2763-2.

Peings, Y., E. Brun, V. Mauvais, and H. Douville, 2013: How stationary is the relationship between Siberian snow and Arctic Oscillation over the 20th century? Geophysical Research Letters 40, 183–188, doi:10.1029/2012GL054083

Rayner, N.A., D.E. Parker, E.B. Horton, and coauthors, 2003: Global analyses of sea surface temperature, sea ice, and night marine air temperature since the late nineteenth century. Journal of Geophysical Research 108: 4407, doi: 10.1029/2002JD002670.

Riddle, E.E., A.H. Butler, J.C. Furtado, J.L. Cohen, and A. Kumar, 2013: CFSv2 ensemble prediction of the wintertime Arctic Oscillation. Climate Dynamics **41**, 1099–1116.

Scaife, A.A., and coauthors, 2014: Skilful long-range prediction of European and North American winters. Geophysical Research Letters **41**: 2514–2519, doi:10.1002/2014GL059637.

Serreze, M.C., and R.G. Barry, 2005: The Arctic Climate System. Cambridge University Press: Cambridge, UK.

Shin, S.H., 2014: Predictability of the East Asian Winter Monsoon by the APCC Multi-Model Ensemble Forecast System. Annual Report APCC, 2014 (in Korean).

Sun, B.M., and C.Y. Li, 1997: Relationship between the disturbances of East Asian trough and tropical convective activity in boreal winter. Chinese Science Bulletin **42**: 500–504.

Sun, J., and J.B. Ahn, 2014: Dynamical seasonal predictability of the Arctic Oscillation using a CGCM. International Journal of Climatology **35**: 1342–1353, doi: 10.1002/joc.4060.

Thompson, D.W.J., and J.M. Wallace, 1998: The Arctic oscillation signature in wintertime geopotential height and temperature fields. Geophysical Research Letters **25**: 1297–1300.

Thompson, D.W.J., and J.M. Wallace, 2000: Annular modes in the extratropical circulation. Part I: month to month variability. Journal of Climate **13:** 1000–1016.

Wang, B., B. Xiang, and J.Y. Lee, 2013: Subtropical High predictability establishes a promising way for monsoon and tropical storm predictions. *Proceedings of the National Academy of Sciences*, **110**, 2718-2722, doi:10.1073/pnas.1214626110

Wang, B., Z. Wu, C.P. Chang, J. Liu, J. Li, and T. Zhou, 2010: Another look at interannual-to-interdecadal variations of the East Asian winter monsoon: The northern and southern temperature modes. Journal of Climate **23**, 1495-1512

Wang, L., and W. Chen, 2010: Downward Arctic Oscillation signal associated with moderate weak stratospheric polar vortex and the cold December. Geophysical Research Letters **37**: L09707, doi: 10.1029/2010GL042659.

Wang, L., W. Chen, and R. Huang, 2008: Interdecadal modulation of PDO on the impact of ENSO on the East Asian winter monsoon. Geophysical Research Letters **35**: L20702, doi: 10.1029/2008GL035287.

Wang, L., W. Chen, W. Zhou, and R. Huang, 2009: Interannual variations of East Asian trough axis at 500 hPa and its association with the East Asian winter monsoon pathway. Journal of Climate **22**: 600–614.

Watanabe, M., and T. Nitta, 1999: Decadal change in the atmospheric circulation and associated surface climate variations in the Northern Hemispheric winter. Journal of Climate **12**: 494–510.

Whitaker, J.S., G.P. Compo, X. Wei, and T.M. Hamill, 2004: Reanalysis without radiosondes using ensemble data assimilation. Monthly Weather Review **132**: 1190–1200.

Wilks DS. 1995. Statistical Methods in the Atmospheric Sciences. Second Edition. Elsevier Academic Press: San Diego, CA.

WMO (World Meteorological Organization), 2012: Manual on the Global Data-Processing and Forecasting System. Volume I – Global Aspects, Updated in 2012. WMO-No. 485, Geneva, Switzerland.

APPENDIX 1. PREDICTION TECHNIQUES

We performed the following two types of predictions:

- Predictions of future series values for Korean average temperature values, circulation index values, and principal component values;
- Predictions of a future field of values for fields of Korean and East Asia gridded temperatures.

Predictands and predictors in the following sections are represented by anomalies in respect to the training period mean values.

A1.1. Prediction of a Future Series Value

Prediction of a future series value is performed by means of multiple regression:

$$y_t = b_0 + \sum_{k=1}^{K} b_k x_{k,t} + \varepsilon_t \qquad (A1.1)$$

where y_t is predictand at time t, $x_{k,t}$ is k-predictor at time t, ε_t is error at time t. Accounting to the size of real available training series of 25 – 30 years, the number of predictors K should not exceed two.

Predictand is a target variable, in our case it is temperature averaged over South Korea or Korean Peninsula, or principal component(s) of temperature fields decomposed by means of Principal Component Analysis (PCA).

Predictor(s) are estimated based on the training period relationships by projecting the predictor variable fields onto correlation map between the predictand and predictor variable fields. This method with some variations has been being utilized in statistical forecast models for decades. Now it is widely applied in downscaling procedures (e.g., Kug et al., 2008; Min et al., 2011; Kryzhov, 2012). This method is applied by Lee et al. (2013a) in “Predictable Modes” statistical forecasting technology which marked a recovery of the physical-empirical approach to long

range forecasting. The main difference between the developed method and the methods mention above is the absence of any restrictions on the correlation map values which provides higher flexibility in construction of the predictors.

The prediction procedure consists of five steps.

On the first step, we compute a correlation map of October predictor fields z and the DJF target variable y series using the data from the training period of size T years:

$$r_{k,s} = \frac{\sum_{t=1}^{T} z_{k,s,t} y_t}{(\sum_{t=1}^{T} z_{k,s,t}^2 \sum_{t=1}^{T} y_t^2)^{0.5}}, \qquad (A1.2)$$

Where s is space (gridpoint) counter

On the second step, we construct T-year long series of predictor(s), computed as a projection of the October predictor(s) anomaly fields on the correlation map.

$$x_{k,t} = \sum_{s=1}^{S} r_{k,s} z_{k,s,t} \qquad (A1.3)$$

If we use multiple regression, i.e., a set of predictors, the first and the second steps are performed for each k-predictor separately.

On the third step, we derive a regression equation by means of Least Squares Estimation (minimizing mean squared error ε) based on the T-years training period.

The fourth is estimation of the (T+1)th year predictor(s) $x_{k,T+1}$ by projecting of the October predictor variable(s) field(s) from the (T+1)th year onto the (corresponding) correlation map(s).

$$x_{k,T+1} = \sum_{s=1}^{S} r_{k,s} z_{k,s,T+1} \qquad (A1.4)$$

The fifth step is estimation of the forecast value of the DJF target variable using

the (T+1)th year value(s) of the predictor(s).

$$y_{T+1} = b_0 + \sum_{k=1}^{K} b_k x_{k,T+1} \qquad \text{(A1.5)}$$

Peculiarity of the method we apply resides in no use of any restrictions on correlation values. In such approach a predictor time series becomes collinear to expansion coefficient series obtained by SVD of a correlation matrix equal to the corresponding correlation map. It makes the method flexible.

A1.2. Prediction of a Future Field of Values

Prediction of temperature (or any other variable) anomaly fields $y_{s,t}$, with *s* and *t* being space and time counters, correspondingly, consists of three stages:

- EOF decomposition of the predictand fields $y_{s,t}$ from the training period of size T;
- Prediction of future values of the truncated PCs, $p_{m,T+1}$, i.e., prediction of the future series value described above;
- Composition of the forecast year predictand field, $y_{s,T+1}$.

EOF decomposition of the predictand fields $y_{s,t}$.

$$y_{s,t} = \sum_{m=1}^{M} e_{s,m} p_{m,t} \qquad \text{(A1.6)}$$

$e_{s,m}$ is mth eigenvector value at point s;

$p_{m,t}$ is mth PC value at time t.

For our purposes, i.e., prediction of PC(s) with further construction of the predicted fields, convenient is to have normalized (standardized) unitless series of PCs with units in EOFs:

$$p_m \sim N(0,1) \qquad \text{(A1.7)}$$

$$\sum_{s=1}^{S}(e_{s,m})^2 = \lambda_m, \qquad \text{(A1.8)}$$

where λ_m is **m**th eigenvalue.

The second stage is prediction of the (**T**+1)th value of each truncated **m**th PC $p_{m,T+1}$ following Eqs. A1.1 – A1.5.

The third stage is composition of the future field of the target variable $y_{s,T+1}$:

$$y_{s,T+1} = \sum_{m=1}^{M} e_{s,m} p_{m,T+1} \qquad \text{(A1.9)}$$

Consistency of the variances of the predicted EOF modes ($e_{s,m} p_{m,T+1}$) is provided by keeping of the condition of Eq. A1.8.

Since the standard deviation of p_m training period series is one, the weight of each predicted EOF modes in amplitude of $y_{s,T+1}$ is equal to $e_{s,m}$ multiplied by correlation coefficient between observed and "reconstructed" y_s during the training period.

APPENDIX 2. VERIFICATION ASSESSMENTS

Verification assessments were performed for each variable and each gridpoint.

Predictand and predictors in the following sections are represented by anomalies in respect to the training period mean values.

A2.1. Verification Strategies

Verification assessments are based on retrospective predictions. Performance of the forecasts is assessed by a Mean Square Skill Score (MSSS), with reference forecasts being climatological ones (Murphy, 1988), and a temporal unadjusted correlation (congruence) coefficient (TCC) also known as an anomaly correlation coefficient.

Murphy (1988) discusses four verification strategies based on the climatological forecast. Two of them are applicable to real-time forecasts. Those two correspond to the cases III (single-valued external climatology) and IV (multiple-valued external climatology) of Murphy (1988). Case III is recommended by WMO (WMO, 2010) and is based on the normals (climatology) from a basic period appointed by WMO and renewed each 30 years. Particularly, officially valid are the normals from the 1961-1990 period (now, the normals from 1981-2010 are also applicable) which are to be replaced with the normals from 1991-2020 in due time. However, on the background of the “global change” the skill of forecasts with the use of so old normals appears overestimated.

Another strategy for real-time forecasts, Case IV of Murphy (1988), implies climatology specified for each particular forecast. For example, climatology from a training period preceding a year of forecast.

Cases I (single-valued internal climatology) and II (multiple-valued internal climatology) are “hypothetical” (Murphy, 1988). They cannot be realized in real-time forecasts. Nevertheless, verification following Case II, which implies verification of cross-validated forecasts, makes sense for extended assessments of new forecast methods.

We assessed our forecasts using strategies II, III, IV. Since verification scores using single-valued external climatology from 1958 – 1983 (Case III) appear overestimated, at least essentially exceeding those from Case IV, we show in the report the results based on climatological forecasts estimated according to Case IV (real-time forecasts with climatologies from the 25-year training periods preceding years of forecasts) and Case II (three-leave-out cross-validated forecasts for the period 1989-2013).

A2.2 Verification Metrics

Detailed descriptions of verification metrics and their applications could be found in the papers (e.g., Murphy, 1988), textbooks on statistical applications in climatology (e.g., Wilks, 1995), WMO documents (e.g., WMO, 002).

A2.2.1 Mean Squared Skill Score

In the following Equations y denotes observations, f - forecasts. In terms of anomalies, y is anomaly in respect to y mean value from the reference period; f is anomaly in respect to the same y mean value from the reference period:

$$\bar{y}_t = \frac{1}{N}\sum_{i=1}^{N} y_{t,i}, \qquad (A2.1)$$

where N is the size of the reference period.

T is the number of years of forecasts and corresponding reference periods, with t being a time counter.

Mean Squared Skill Score (*MSSS*) is estimated as

$$MSSS = \frac{MSE - MSE_c}{MSE_c} \qquad (A2.2)$$

Where Mean Squared Error (*MSE*) of the tested forecasts is

$$MSE = \frac{\sum_{t=1}^{T}(f_t - y_t)^2}{T} \qquad (A2.3)$$

and Mean Squared Error of climatological forecasts (*MSEc*) is

$$MSE_c = \frac{\sum_{t=1}^{T}(cf_t - y_t)^2}{T} \qquad (A2.4)$$

where *cf* is a climatological forecast value – the climatology from the reference period:

$$cf_t = \bar{y}_t$$

In terms of anomalies $cf_t = 0$ for all *t*s.

MSSS varies within minus infinity to +1.

MSSS = +1 indicates to perfect forecasts.

MSSS = 0 indicates to equality of the *MSE* s of tested and climatological forecasts (no skill threshold).

MSSS < 0 indicates to unskilled forecasts.

A2.2.2. Temporal (Anomaly) Correlation Coefficient

Temporal (anomaly) correlation coefficient (*TCC*) in the case of verification is estimated as an unadjusted correlation or congruence coefficient:

$$TCC = \frac{\sum_{t=1}^{T}(f_t - cf_t)(y_t - \bar{y}_t)}{\sqrt{\sum_{t=1}^{T}(f_t - cf_t)^2 \sum_{t=1}^{T}(y_t - \bar{y}_t)^2}} \qquad (A2.5)$$

All the notations are as in the *MSSS* section above.

Research Report 2015–09

DEVELOPMENT OF PHYSICAL-EMPIRICAL MODELS FOR SEASONAL PREDICTIONS OF WINTERTIME CLIMATE VARIABLES OVER EAST ASIA

Vladimir Kryjov

APCC
APEC CLIMATE CENTER

APEC Climate Center
12 Centum 7-ro, Haeundae-gu, Busan 48058, Republic of Korea
Tel: +82-51-745-3900 Fax: +82-51-745-3949

www.apcc21.org

9 791156 981084 93550
ISBN 979-11-5698-108-4